ACT Government
Chief Minister, Treasury and Economic Development

Freedom of Information Publication Coversheet

The following information is provided pursuant to section 28 of the *Freedom of Information Act 2016*.

FOI Reference: CMTEDDFOI 2021-316

Information to be published	Status
1. Access application	Published
2. Decision notice	Published
3. Documents and schedule	Published
4. Additional information identified	No
5. Fees	Waived
6. Processing time (in working days)	15
7. Decision made by Ombudsman	N/A
8. Additional information identified by Ombudsman	N/A
9. Decision made by ACAT	N/A
10. Additional information identified by ACAT	N/A

From: no-reply@act.gov.au
To: CMTEDD FOI
Subject: Freedom of Information request
Date: Thursday, 11 November 2021 3:15:49 PM

Please find online enquiry details below. Please ensure this enquiry is responded to within fourteen working days.

Your details

All fields are optional, however an email address OR full postal address must be provided for us to process your request. An email address and telephone contact number will assist us to contact you quickly if we need to discuss your request.

Title:
First Name:
Last Name:
Business/Organisation:
Address:
Suburb:
Postcode:
State/Territory:
Phone/mobile:
Email address:

Request for information

(Please provide as much detail as possible, for example subject matter and relevant dates, and also provide details of documents that you are not interested in.)

Under the Freedom of Information Act 2016 I want to access the following document/s (*required field):

We are a group of researchers at [redacted] who would like to draw lessons learned from past procurement failures. We would like to access information about the RAAF Fairbairn hangar roof collapse in Canberra in 2003. We haven't found any public domain investigation report, so would like to access any documentation on this accident. Thank you in anticipation.

I do not want to access the following documents in relation to my request::

Thank you.
Freedom of Information Coordinator

ACT Government
Chief Minister, Treasury and Economic Development

Our ref: CMTEDDFOI 2021-316

[redacted]

FREEDOM OF INFORMATION REQUEST

I refer to your application under section 30 of the *Freedom of Information Act 2016* (the Act), received by the Chief Minister, Treasury and Economic Development Directorate (CMTEDD) on 11 November 2021.

Specifically, you are seeking: *"The final investigation report about the RAAF Fairbairn hangar roof collapse in Canberra in 2003."*

Authority

I am an Information Officer appointed by the Director-General under section 18 of the Act to deal with access applications made under Part 5 of the Act.

Timeframes

In accordance of section 40 of the Act, CMTEDD was required to provide a decision on your access application by 9 December 2021.

Decision on access

Searches were completed for relevant documents and one document was identified that falls within the scope of your request.

I have decided to grant full access to the relevant document. The document released to you is provided as **Attachment A** to this letter.

Charges

Pursuant to *Freedom of Information (Fees) Determination 2018* processing charges are applicable for this request because the total number of pages to be released to you exceeds the charging threshold of 50 pages. However, I have decided to waive the charges in this specific instance.

Online publishing – Disclosure Log

Under section 28 of the Act, CMTEDD maintains an online record of access applications called a disclosure log. Your original access application, my decision and documents released to you in response to your access application will be published in the CMTEDD

disclosure log after 3 days after the date of my decision. Your personal contact details will not be published. You may view CMTEDD disclosure log at https://www.cmtedd.act.gov.au/functions/foi.

Ombudsman Review

My decision on your access request is a reviewable decision as identified in Schedule 3 of the Act. You have the right to seek Ombudsman review of this outcome under section 73 of the Act within 20 working days from the day that my decision is published in CMTEDD disclosure log, or a longer period allowed by the Ombudsman.

We recommend using this form *Applying for an Ombudsman Review* to ensure you provide all of the required information. Alternatively, you may write to the Ombudsman at:

The ACT Ombudsman
GPO Box 442
CANBERRA ACT 2601

Via email: actfoi@ombudsman.gov.au

ACT Civil and Administrative Tribunal (ACAT) Review

Under section 84 of the Act, if a decision is made under section 82(1) on an Ombudsman review, you may apply to the ACAT for review of the Ombudsman decision. Further information may be obtained from the ACAT at:

ACT Civil and Administrative Tribunal
Level 4, 1 Moore St
GPO Box 370
Canberra City ACT 2601
Telephone: (02) 6207 1740
http://www.acat.act.gov.au/

Should you have any queries in relation to your request please contact me by telephone on 6207 7754 or email CMTEDDFOI@act.gov.au.

Yours sincerely

Katharine Stuart
Information Officer
Information Access Team
Chief Minister, Treasury and Economic Development Directorate

2 December2021

Connell Mott MacDonald

...building the future

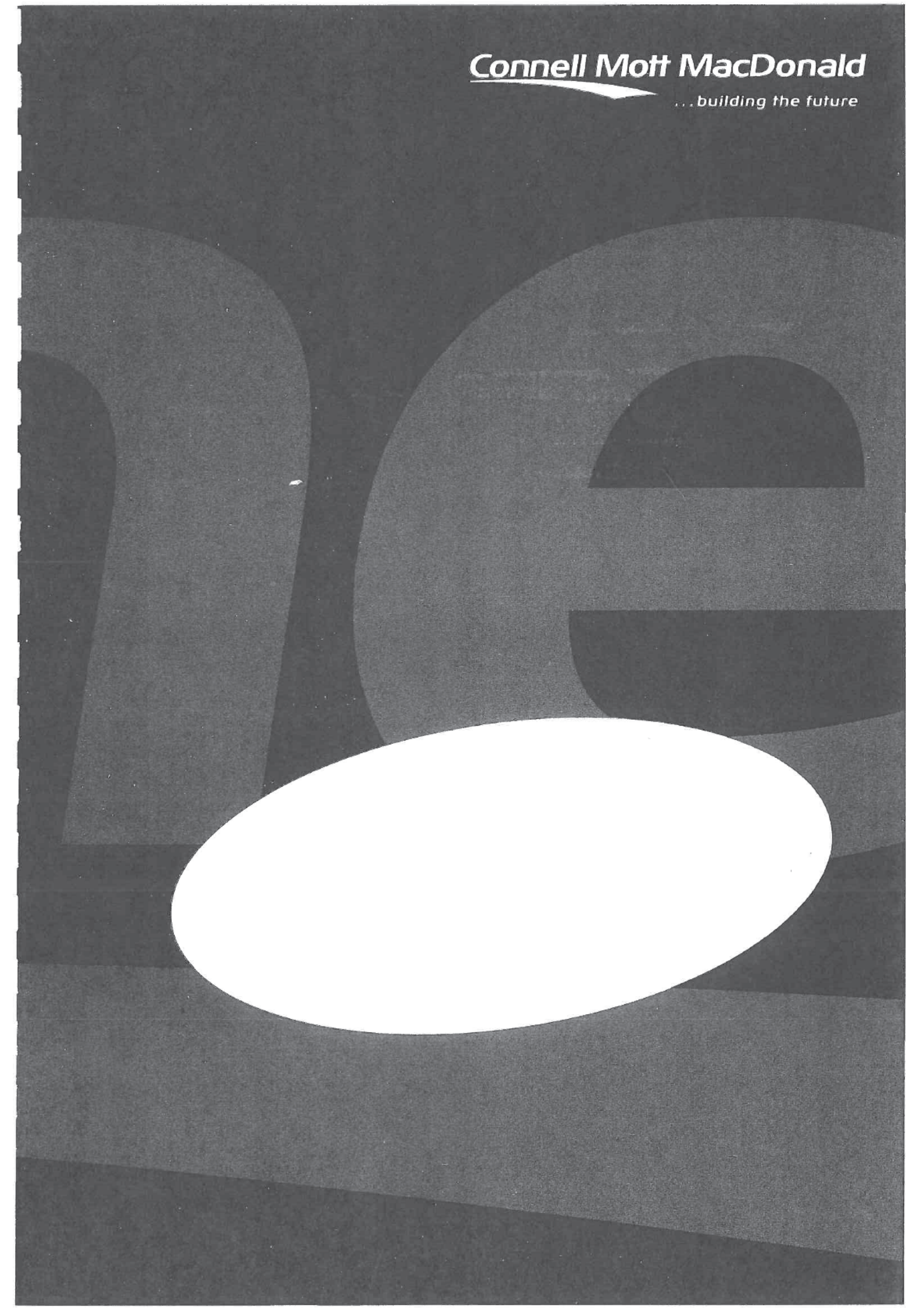

Connell Wagner Pty Ltd
ABN 54 005 139 873
116 Military Road
Neutral Bay
New South Wales 2089 Australia

Telephone: +61 2 9465 5555
Facsimile: +61 2 9465 5598
Email: cwsyd@conwag.com
www.conmottmac.com

Strarch Hangar Collapse
Final Investigation Report

12 October 2004
Reference C059 S1 SA
Revision 2

Connell Mott MacDonald
...building the future

Document Control

Connell Mott MacDonald ...building the future

Document ID: S:\C059.S1.SA\ENG\STRUCT\FINAL REPORT JUNE 04\FINAL REPORT OCTOBER 04.DOC

Rev No	Date	Revision Details	Typist	Author	Verifier	Approver
0	8-9-03	Preliminary report	WS	WS/KK	BRS	JFW
1	2-7-04	Draft final report including UWS testing	WS	WS/KK	BRS	JFW
2	12-10-04	Final report including UWS testing	WS	KK/WS	BRS	JFW

Table of Contents

1. Introduction

Connell Mott MacDonald was engaged by ACT Work Cover to investigate the cause of collapse of a partially constructed aircraft hangar building structure for the Special Purpose Aircraft Facility (SPAF) located at RAAF Fairburn, Canberra. The SPAF was being constructed by Construction Control with the design, erection methodology and construction of the hangar superstructure subcontracted to Strarch International (Strarch International 2003a p9).

The hangar structure consists of eight planar frames positioned along the 77.4m length of the building at centre-to-centre distances of either 8m or 11.75m. Each frame is made of a primary truss approximately 4m deep spanning 95m between two tapered trussed legs. The frames are connected by secondary distribution trusses and purlin trusses spanning between them. The hangar structure is built using a proprietary stress-erection technology. This technology utilises a high strength steel tendon (consisting of 12 x 7 wire strands, similar to that used in a prestressed concrete beam – strand nominal diameter =15.2mm, strand Minimum Breaking Capacity = 250 kN) installed inside the tubular bottom chord of each primary truss. Each planar frame is fabricated in segments and assembled in an unstressed state on support scaffolds.

The normal construction methodology is such that the roof sheeting is installed on the frames whilst they are still resting on their scaffold supports in the unstressed state. Following the completion of roof sheeting process the structure is erected by tensioning the tendon ("cable") that runs through the discontinuous tubular lower chord of the roof truss. The tensioning process progressively closes up the gaps in the lower chord, lifting the entire frame upwards. This process is followed initially until the "lift-off" of the frames from the support scaffolds (at which point the scaffolds are removed) and then until the fully erected state is achieved (Strarch International 2003a p9).

In the instance of the SPAF hangar it has been reported (Strarch International 2003a p11) that difficulties were being experienced with the application of roof sheeting to the unstressed structure, due to the lack of camber on the frames. To facilitate the completion of the roof sheeting process and allow unimpeded access for ground level work under the structure it was decided to stress-erect the structure to the point at which it had just lifted off from the support scaffolds. The frames were fully lifted off from the support scaffolds on 23/4/03 (Strarch International 2003a p14). Roof sheeting progressed after this date and 3.5 bays of roof cladding had been completed on 7/5/03 (Strarch International 2003a p11) and Figure A1. The structure collapsed at 11.52 am on the same day, injuring several workers (Strarch International 2003a p14).

Temporary members are fitted to the structure during the erection process. Referred to as "gap locks" these are located between the discontinuous sections of the bottom chord and act to prevent the gaps between the bottom chord sections from opening up during the stress erection process. The gap locks limit "reverse curvature" of the central sections of the partially erected roof truss (Strarch International 2003b p68).

This final report describes the analytical work undertaken by Connell Mott MacDonald and the component testing conducted by the University of Western Sydney in an effort to ascertain the cause of the structure collapse. The report is arranged in several parts as follows:

- A description of the analytical model used to simulate the performance of the structure; the material properties used, member properties, boundary conditions and analysis method are described.
- A description of the analysis results obtained and summary of the results from testing of gap lock components (the full test report is in Appendix C).
- Conclusions drawn from examination of the model results and University of Western Sydney gap lock test results.

2. The Model

2.1 Software Used

ANSYS general-purpose finite element analysis (FEA) program has been used for the analytical studies presented in this report. This software simulates the performance of structural elements under defined loading and boundary conditions. ANSYS is one of the World's most advanced and reputable FEA programs and is used widely throughout many industries.

2.2 Model Description

A model was constructed to simulate the performance of Frame 6 of the Canberra SPAF Hangar structure. This frame was chosen, as the loads on the frame were relatively high due to the weight of the roof sheeting it supported. Also this frame appears to be one of the first two frames to have collapsed based on eyewitness accounts (Strarch International 2003b p51). This is also supported by the position of the collapsed structure that shows Frames 6 & 7 sitting lower than the other frames. The model geometry, member nomenclature and the orientation of the global axes are shown in Figure 1 of this report.

The finite element method relies on the use of elements, single mathematical representations of small parts of the structure, and nodes, the locations at which these structural elements are joined together. Mathematically the elements that make up the model are combined to represent the performance of the entire structure.

The model is based upon the use of line elements, either beam elements or link elements. Although these elements appear as lines graphically, the properties embodied in the element represent the performance of the actual three-dimensional members of the structure. Initially the model is constructed in the as-assembled state. This includes the support scaffolds on which the structure is assembled prior to pre-tension of the lower chord. These support scaffolds are shown in red in Figure 1.

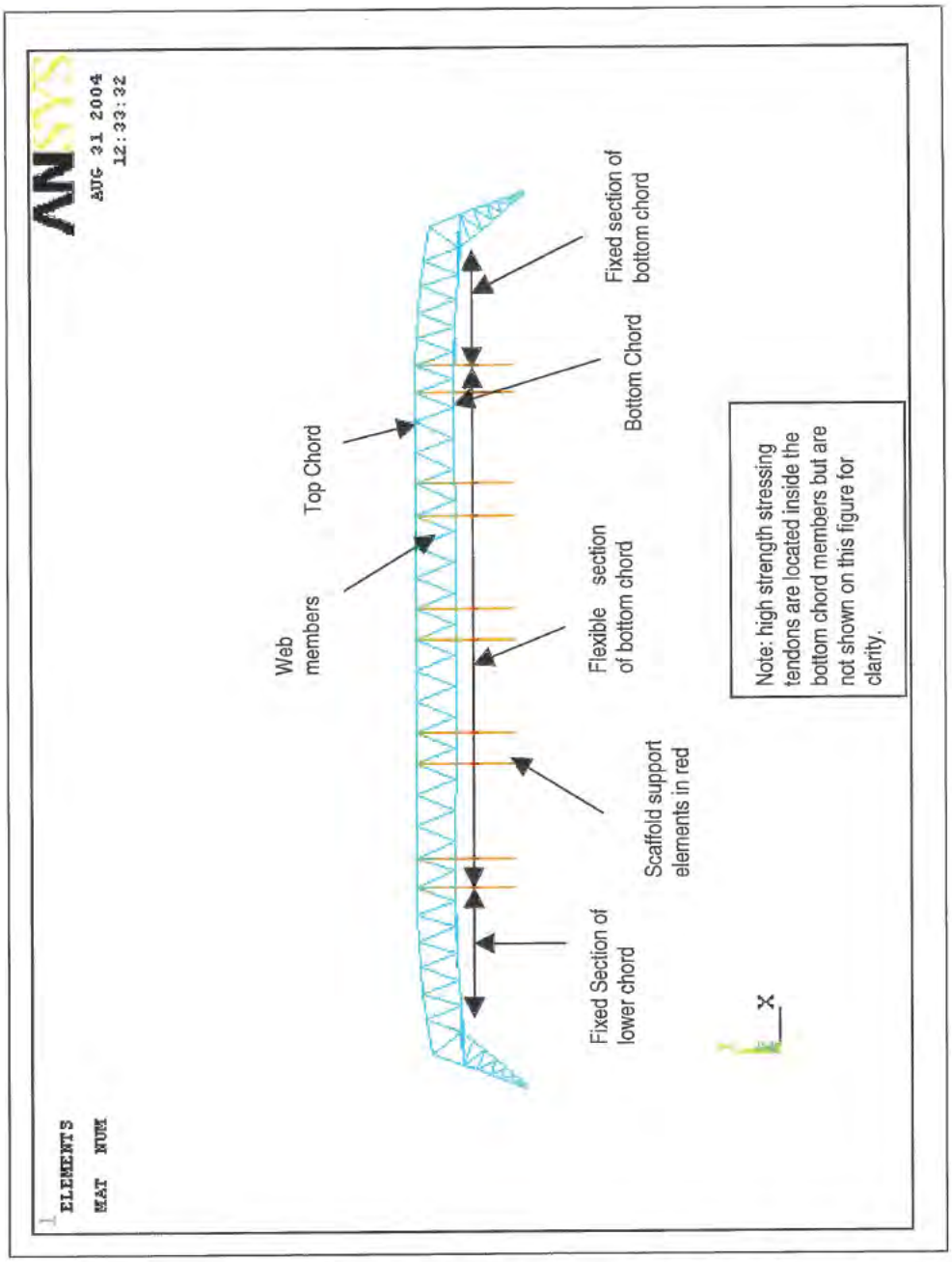

Figure 1 Model constructed to simulate the performance of the SPAF Hangar Frame 6

2.3 Material Properties

The material properties used in the model are listed in Table 1.

Table 1 Material properties used in the model.

Property	Material Number 1 (all elements except scaffold supports)	Material Number 2 (scaffold supports)
Elastic Modulus (Pa)	2.00e+11	2.00e+11
Poisson's Ratio	0.25	0.25
Density (kg/m^3)	7850	0*
Thermal Expansion Coefficient (m/m/^{o}C)	1.9e-5	1.9e-5

* Zero density was used for support elements to ensure that when the frame lifted off the supports no influence from the weight of the supports would influence the results. The effect of these elements was removed from the analysis for the third step (refer to section 2.7) so as to allow the model to deflect downwards below the level of the supports.

2.4 Member Properties

The elements used in the analysis embody the structural performance of the actual members used. To simulate this performance several parameters need to be entered into the model. These parameters are listed in Table B1 in Appendix B of this report.

The performance of the lower chord of the Strarch structure is somewhat complex and warrants further explanation. The gaps between the different segments of the discontinuous lower chord in the flexible section of the frame were modelled using "compression-only" elements in ANSYS with an initial strain. This means that these elements are not active structurally until the gaps between adjacent segments have closed up.

In parallel with the lower chord elements, "tension-only" elements were modelled between the lower ends of the web members in the flexible section of the frame. These tension-only elements become inactive when under compression. When under tension these elements simulate the performance of the gap-locks used in the lower chord of the structure. These elements were given a cross-sectional area equivalent to that of the longitudinal plate elements of the gap-lock fittings.

The stressing tendon ("cable") was modelled parallel to and offset below the lower chord and gap lock elements previously described. Link elements were used to represent the cable between the nodes at the intersection of each pair of web elements. These elements were given a cross-sectional area equivalent to the twelve strands that form the cable. Figure 2 indicates the configuration of the lower chord, gap lock and cable elements.

2.5 Boundary Conditions

The failed state/position of the structure indicated an "in-plane" failure mode for the critical frames (Figure A1). For this reason and for computational simplicity it was decided to model the frame as a two-dimensional structure. Section 4 of this report includes a more thorough discussion of possible three-dimensional effects between adjacent frames. Out-of-plane movements (along the Z-axis) and rotations (about the X and Y-axes) at all nodes were restrained to simulate this two-dimensional behaviour.

The right-hand side leg of the structure has been connected at its base as a pin joint, where translations are restricted but rotations (about the Z-axis) are allowed. The left-hand side leg was connected at its base as a sliding joint so that it could not translate in the vertical direction (Y-direction)

but was allowed to translate in the horizontal direction (X-direction) as the structure is stress-erected. This latter condition simulates the performance of the sliding support of the structure. No allowance was made for friction on the sliding support as this was considered to have a relatively minor effect on the overall behaviour of the structure.

2.6 Loading

Three types of external loads were considered in the analysis.

Firstly, gravity loads were applied to allow simulation of the self-weight of the primary structure.

Secondly, dead loads were calculated for secondary steelwork on Frame 6. This includes roof trusses and the distribution trusses connecting adjacent frames. The weights of these elements were apportioned appropriately between the nodes on the top chord of the model and applied as point loads. An upper and lower bound approach was used to calculate these loads.

To obtain the lower bound loads no allowance was made for connections between the members. Also from photographs it appears that some of the secondary steelwork (such as rod bracing between roof trusses and cross bracing at the lower chord) had not been installed at the time of the collapse. The weight of such secondary steelwork was excluded for the lower bound case.

The upper bound loads were obtained by applying a factor of 1.15 to the calculated loads to allow for the additional weight of connections and fittings. This is considered to be a conservative allowance, ie, an overestimate of such additional weights. Also in this case it was assumed that all secondary steelwork indicated on the drawings was present on the structure at the time of collapse.

Thirdly, the weight of the roof sheeting (tertiary structure) was allowed for by a distributed pressure of 0.14 kPa (Strarch International 2003b p60) and again apportioned appropriately between the nodes on the top chord of the model.

No allowance was made for live loading on the structure, in the base model. However, an estimate of the effects of a live loading of 0.25 kPa was made and is discussed in Section 4 (Discussion). It should be noted that the relevant Australian Standard AS1170, requires the roof to be designed to support a live load of 0.25 kPa to cater for maintenance staff, tools and equipment.

Cable pre-tension was applied to the lower cable, inside the truss bottom chord, as an equivalent negative temperature. This acts to contract the elements that make up the lower cable, resulting in an appropriate tension. The boundary condition between the cable and the web elements (Figure 1) at the lower chord warrants further explanation. As the cable tension is applied, relative movement occurs between the cable and the discontinuous lower chord in the flexible section. In reality some friction and binding will occur between the chord members and the cable. The prediction and hence simulation of this friction/binding would be difficult, if not impossible. Instead the cable elements and the web member end nodes have been "coupled" in the vertical (Y-direction). This allows for free sliding in the global horizontal direction whilst ensuring the compatibility of vertical movements between the cable and the lower chord members. This provides a reasonable approximation of the structural behaviour through and just beyond the lift-off stage. For this early stage of the stress-erection of the structure, the near-linear alignment of the bottom chord will mean that the interaction, between the cable and lower chord members, is relatively small.

The "cable" elements are attached by the same Y-direction coupling to the nodes on the lower chord of the fixed section of the structure. At the ends of the "cable" the end nodes of the cable have been merged with the coincident nodes of the structural elements. The locations where these nodes have

been merged coincide with the jacking points at the "dead" and "live" ends of the cable on the actual structure.

Figure 2 depicts the node coupling between the cable and web member nodes at the lower chord. It can be seen that the cable elements have been modelled 50mm below the end of the web member elements to simulate their actual location, running through the lower chord tubular members. The coupling allows relative movement in the horizontal direction (X-direction) between the cable nodes and the web member nodes.

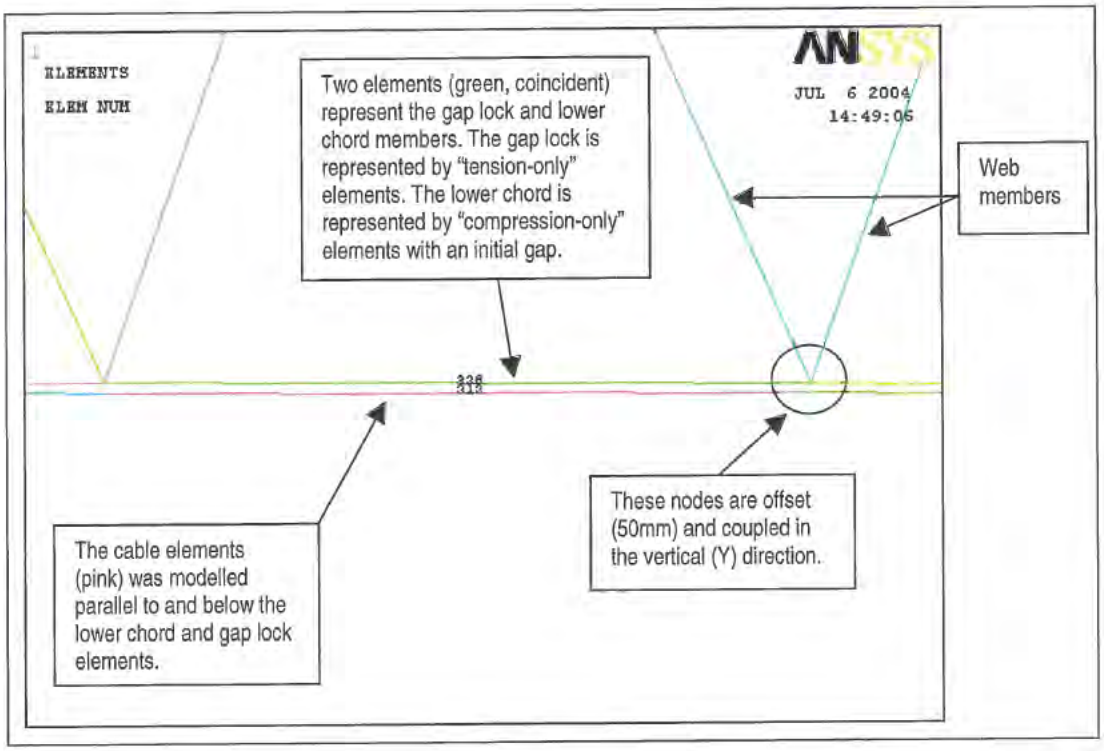

Figure 2 Depiction of node coupling between cable and web member nodes at the lower chord.

2.7 Analysis Method

The actual behaviour of Strarch frame structure during stress-erection is complex and contains a number of sources of non-linear behaviour. It was initially assumed that the period of the stress erection process that is of interest (ie. through to just after "lift-off") would not contain material non-linearity. Therefore, only geometric non-linearities were included in the presented analyses. The adequacy of this assumption was confirmed by the analytical results that indicated no yielding of the top chord material, even at the final load step with all loads applied.

The geometrically non-linear analysis considers large displacement behaviour as the overall load is applied in small steps. As the structure displaces at each load step the stiffness matrix for the structure is updated to represent the state of the structure under the applied load.

The analysis was run in three steps to simulate the actual erection process of the structure.

Firstly the model was run under the self-weight of the frame and the nodal forces from the dead load of the secondary steelwork. The support scaffolds were active during this load step to support the frame. These loads were applied progressively throughout this load step.

Secondly the cable pre-tension was applied to the point at which the frame had lifted off the support scaffolds by approximately 100 mm (at the centre). This was applied progressively as a negative temperature to the cable elements. During this load step the loads applied in the first load step (self-weight and dead loads of secondary steelwork) remained constant.

Thirdly the weight of the roof sheeting (tertiary structure) was progressively applied to the structure without the presence of the support scaffolds. During this third load step the self-weight and cable pre-tension effects are still active. The support elements were rendered inactive for this step.

3. Results

3.1 Model Validation

The performance of the model was checked to ensure that it was behaving as expected. Figures 3 and 4 indicate the displaced shape of the model and the end of the second and third analysis steps.

The model displayed the characteristic M-shape described in Strarch documentation (Strarch International 2003b p67) at the lift off stage (Figure 3). Following the application of roofing loads, with the cable anchorages locked-off, the model displaces below its original position to that shown in Figure 4.

Figure 5 indicates the status (active=1 or inactive=2) of the support elements. The support elements are labelled as Prop1 to Prop10 from the left-hand side of the model. From the figure it can be seen that the outside supports become inactive first, with the centre supports the last to become inactive at t=190s. Prop5 is the last to lift off (t=190s).

It should be noted that the notion of "time" referred to herein simply provides a measure of the gradual application of loads on the structure over each load step, and is not representative of "real" time. For example, the loads for the first load step are applied between t=0 and 100s, the loads of the second load step are applied between t=100s and 200s, and those of the third load step are applied between t=200s and 300s.

Figure 6 indicates the maximum stress levels in the top chord elements at the end of the final load step (t=300s) with all loading applied. The maximum compressive stress calculated was 210 MPa and yield stress for this member is 350 MPa. This indicates that the assumption to exclude non-linear material behaviour from the analysis was valid.

The vertical displacement of the top chord node in the centre of the model is shown in Figure 7. It may be noted that the model centre starts to lift at t=190s in the second load step (tensioning of cable). At the end of the second load step the centre node has lifted roughly 100 mm above its initial position. During the third load step, roofing loads are progressively applied until the node is 290 mm below its initial position at the end of the analysis.

The results reported in the following section are, unless stated otherwise, for the upper bound loads as defined earlier.

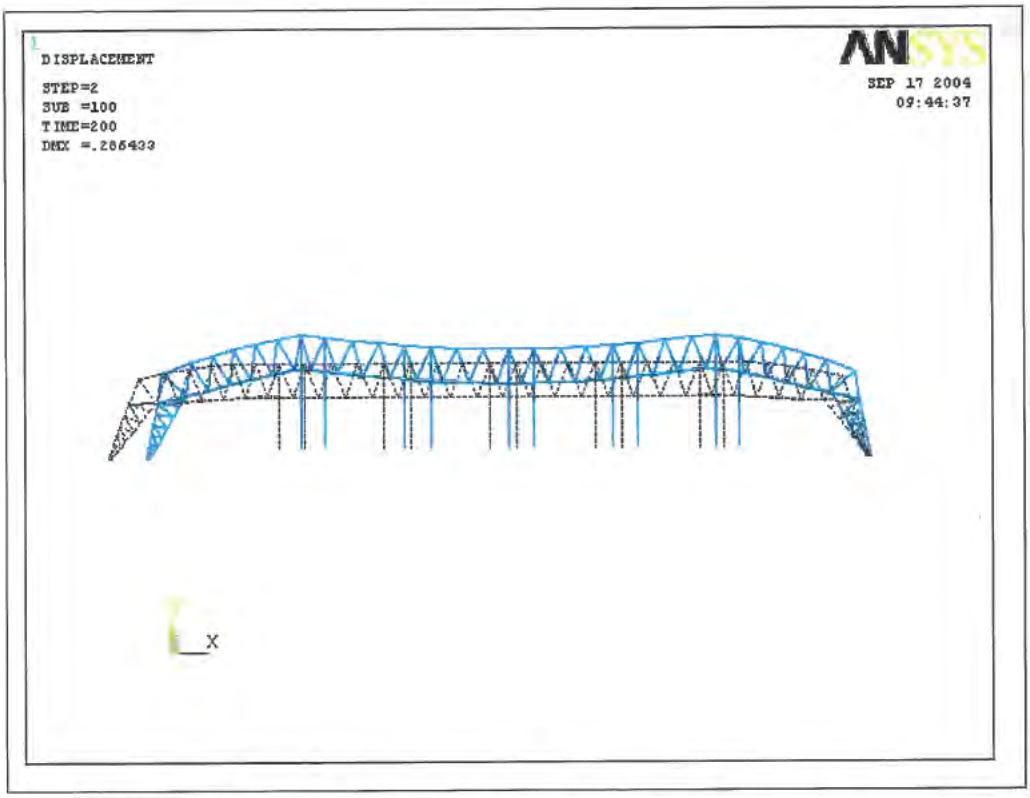

Figure 3 Displaced shape of the model at lift-off *(Note: The plotted displacements have been exaggerated.)*

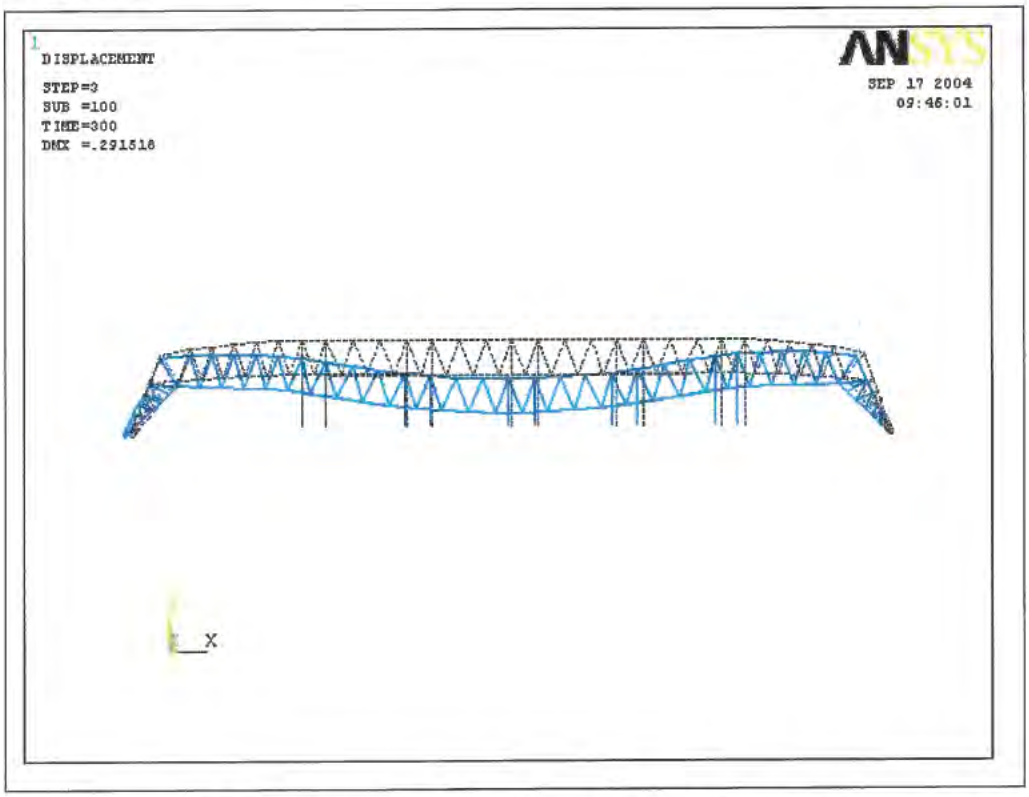

Figure 4 Displaced shape of model at end of third load step *(Note: The plotted displacements have been exaggerated)*

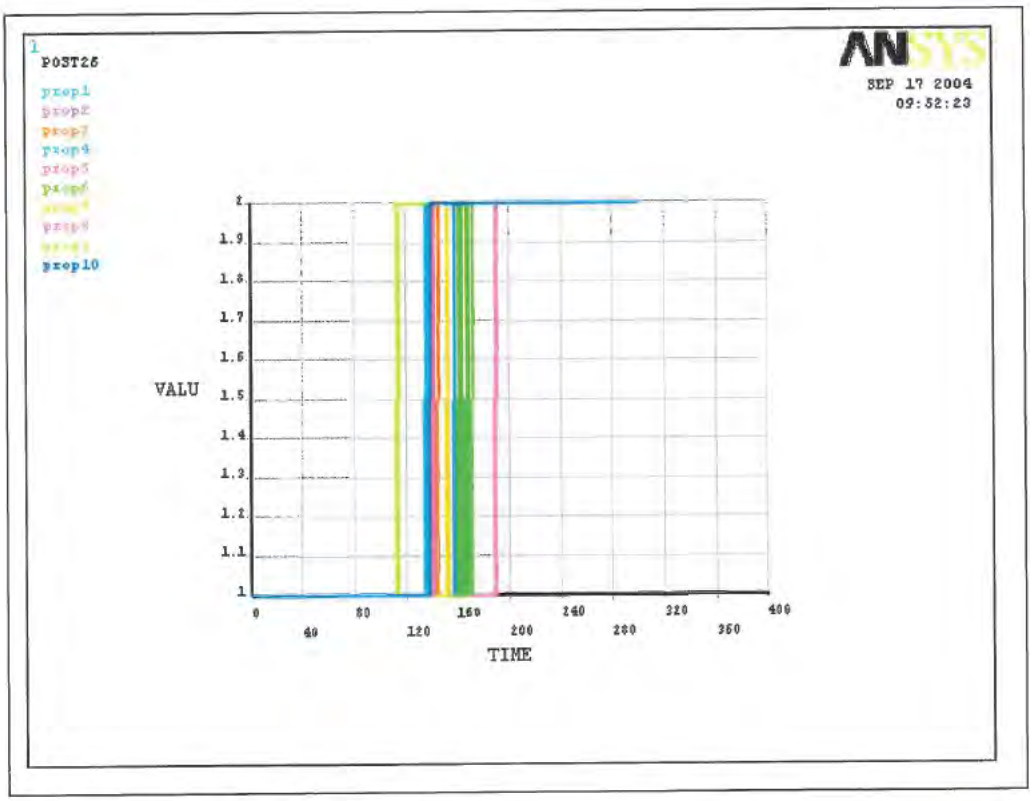

Figure 5: Lift Off status from supports.

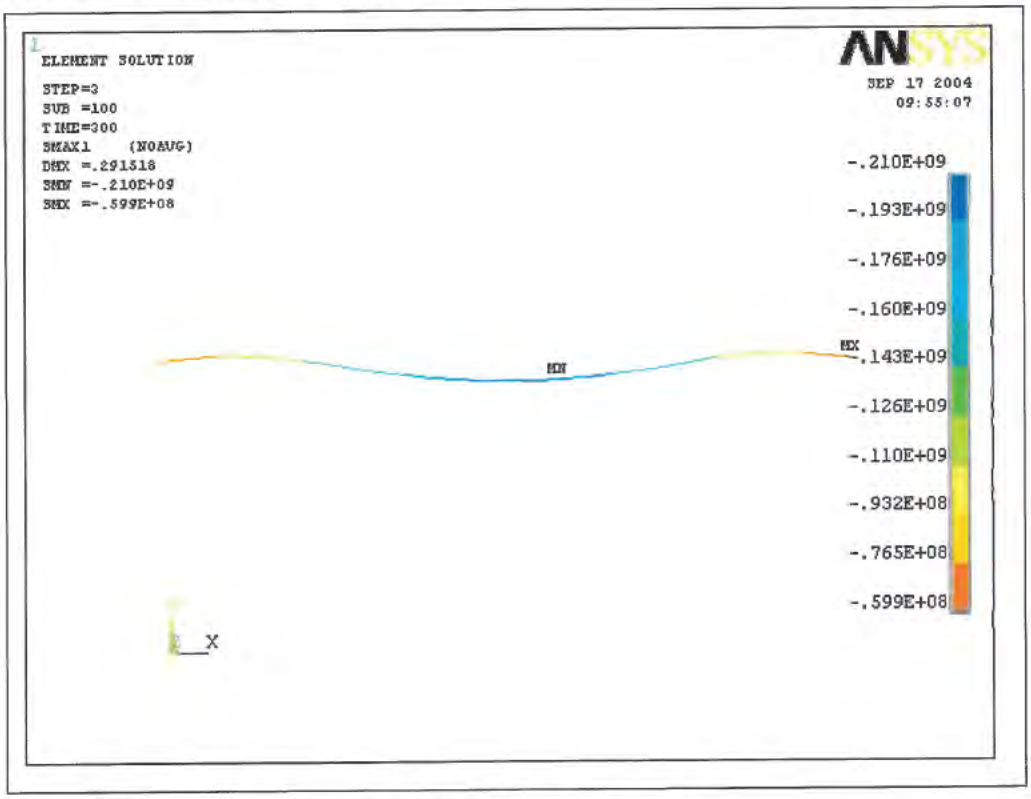

Figure 6: Stress levels in the top chord at the final load step.

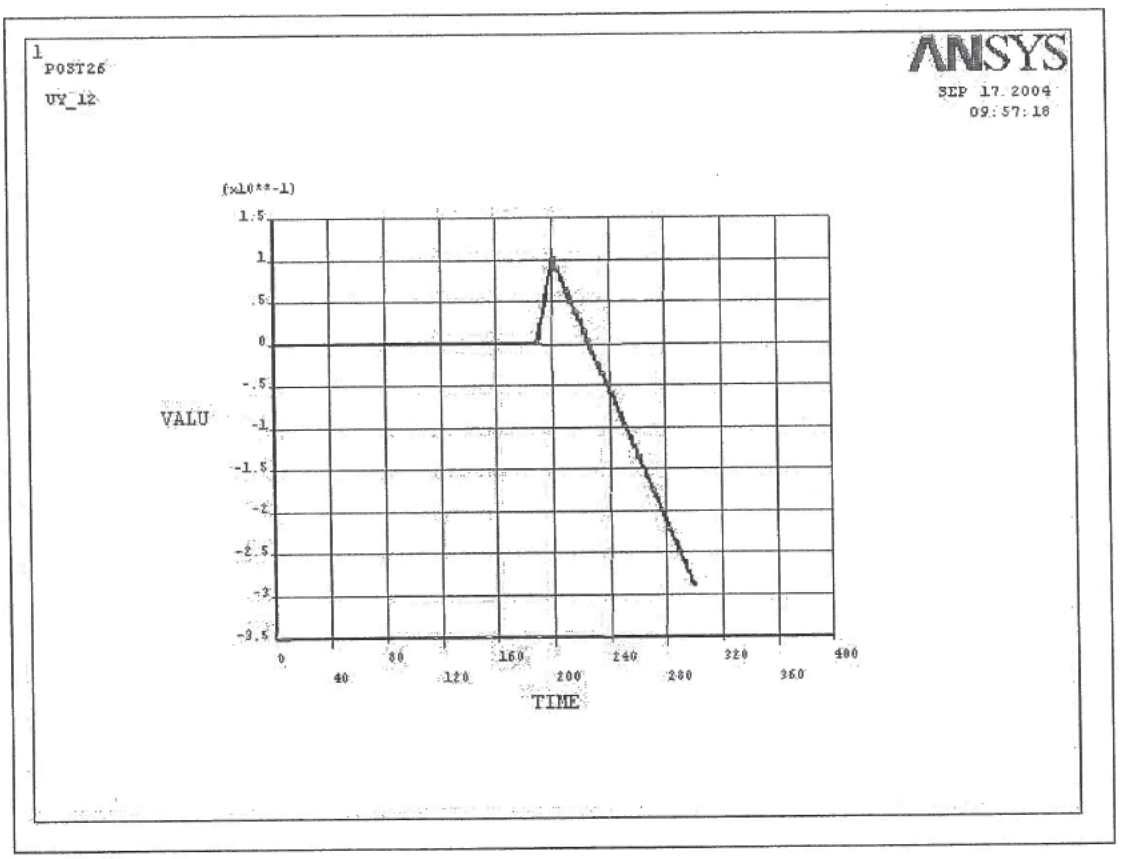

Figure 7: Y direction displacement at the mid-span (y scale +0.15m to -0.35m).

3.2 Cable Tension

Figure 8 indicates the variation of cable tension at the mid-span of the model with time, throughout the analysis. Tension increases to lift-off at t=190 s then remains steady until the roofing loads begin to be applied at t=200 s. At lift-off cable tension is 711 kN and the final cable tension (at the end of step 3 with all roof sheeting loads applied) is 1040 kN. This compares to an expected cable "yield" load of 2550 kN.

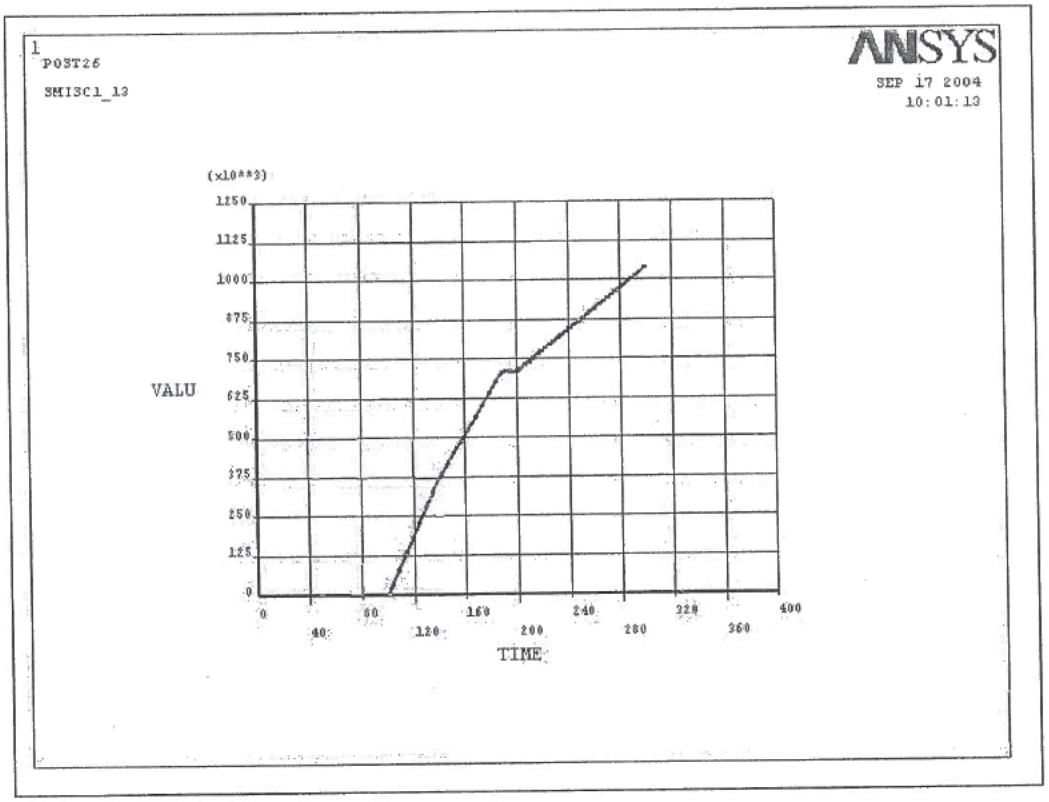

Figure 8: Cable Tension at the mid-span vs Time.

3.4 Gap Lock Loads

As described earlier the gap locks are temporary members installed for erection purposes. They are intended to prevent the gaps in the lower chord of the structure from opening beyond their as-assembled gap.

The gap lock at the centre of the structure was the most highly loaded. The time history of load on this gap lock throughout the analysis is shown in Figure 9. As explained earlier, "time" is merely a proxy value for the ramped application of loads throughout the analysis. At the lift off stage (t=190s) the calculated load in the gap lock was 251 kN. At the end of the analysis, with all roof-sheeting loads applied, the load in the gap lock was 392 kN. For comparison the results with lower bound applied secondary steelwork loads gave a load of approximately 350 kN on the same gap lock.

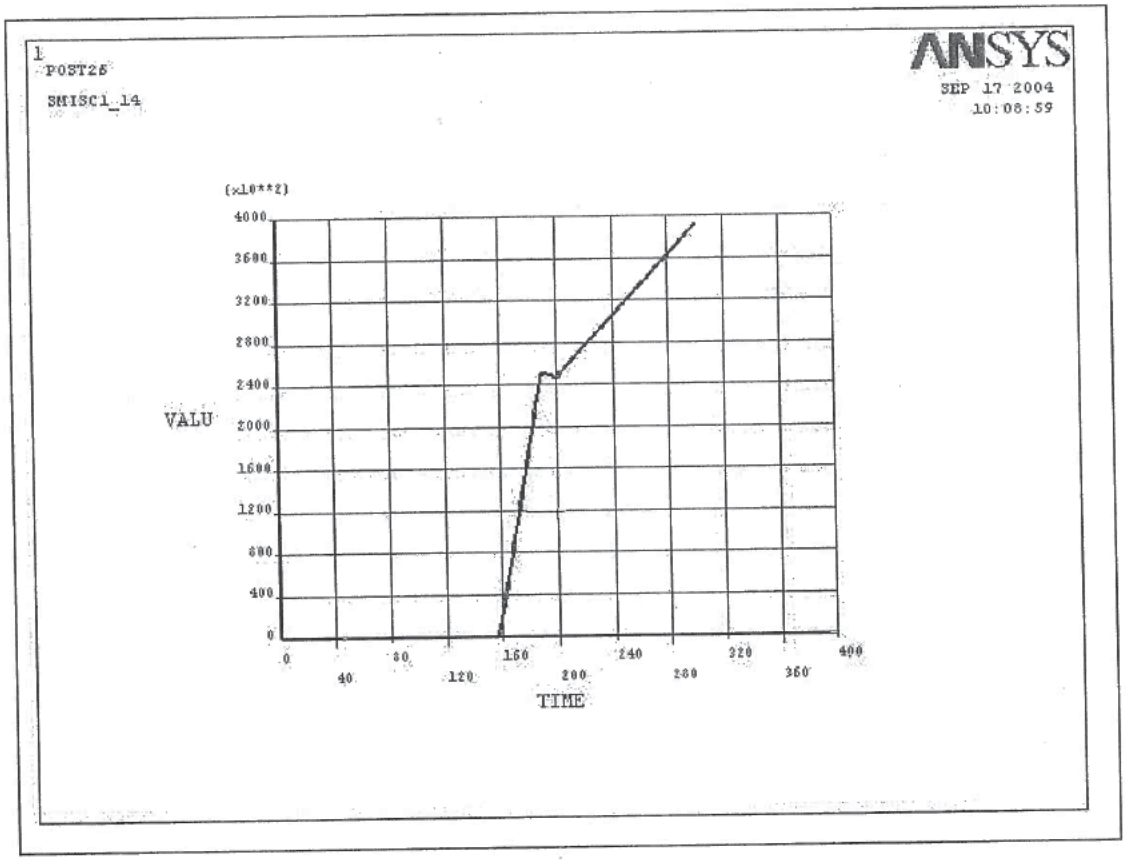

Figure 9: Load in centre gap lock throughout the analysis.

3.5 Stresses in Other Members

Figures 10 and 11 indicate the calculated axial stress levels in the other members of the model at the lift-off and final states, respectively. The most highly stressed members are of grade 350 material in each case, with a yield stress of 350 MPa. The highest calculated stresses in any member were 216 MPa (compression) and 116 MPa (tension) at the end of the analysis.

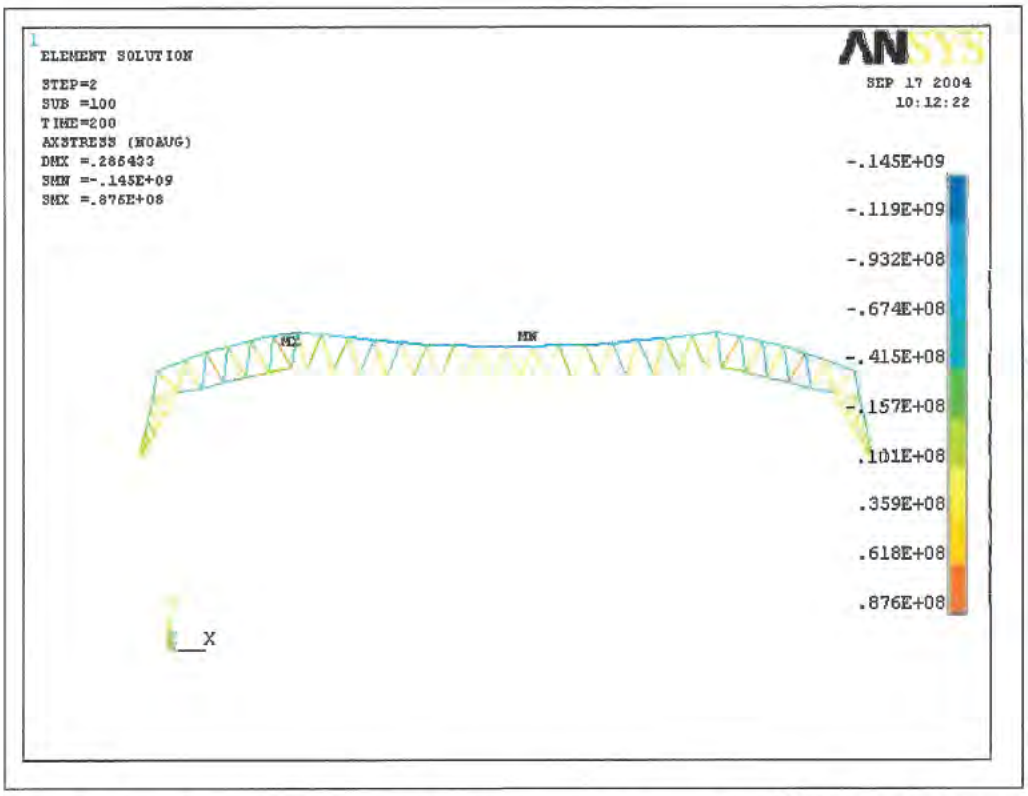

Figure 10: Axial stress at the lift off stage (varying in the range of –146 MPa and 88 MPa)

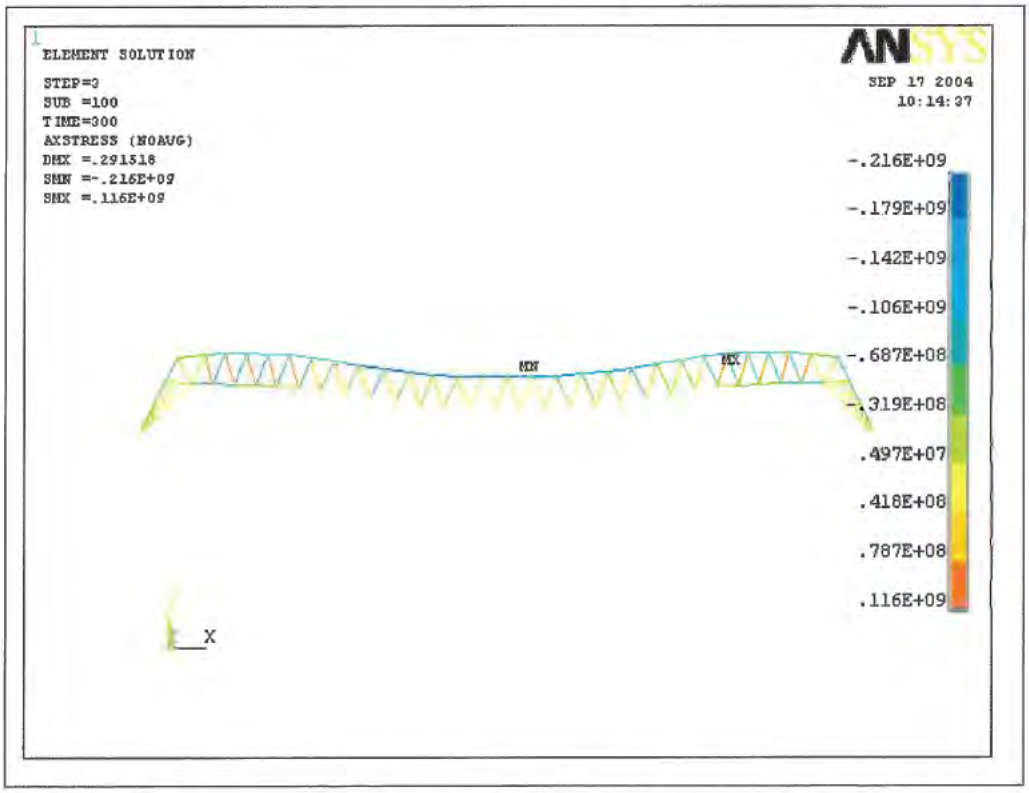

Figure 11: Axial stress at the end of step three, with all roofing loads applied. Stress level varies between -214 MPa and 115 MPa.

3.6 Gap Lock Component Testing

In order to get an accurate understanding of the behaviour and the capacity of the gap lock components in the Strarch structure the NATA accredited laboratory at the University of Western Sydney's Centre for Construction Technology and Research were engaged to conduct a programme of testing. The test report has been included as Appendix C of this document (Wheeler 2004).

The testing involved a total of nine gap lock components, supplied from the failed structure by ACT Work Cover. These gap locks were tested in a range of configurations using a test rig (Figure 12) to simulate the lower chord members adjacent to the gap lock. The parameters varied between tests included the width of the gap lock end plate, the length of bolts used and the geometric relationship between the gap lock and the adjacent lower chord members.

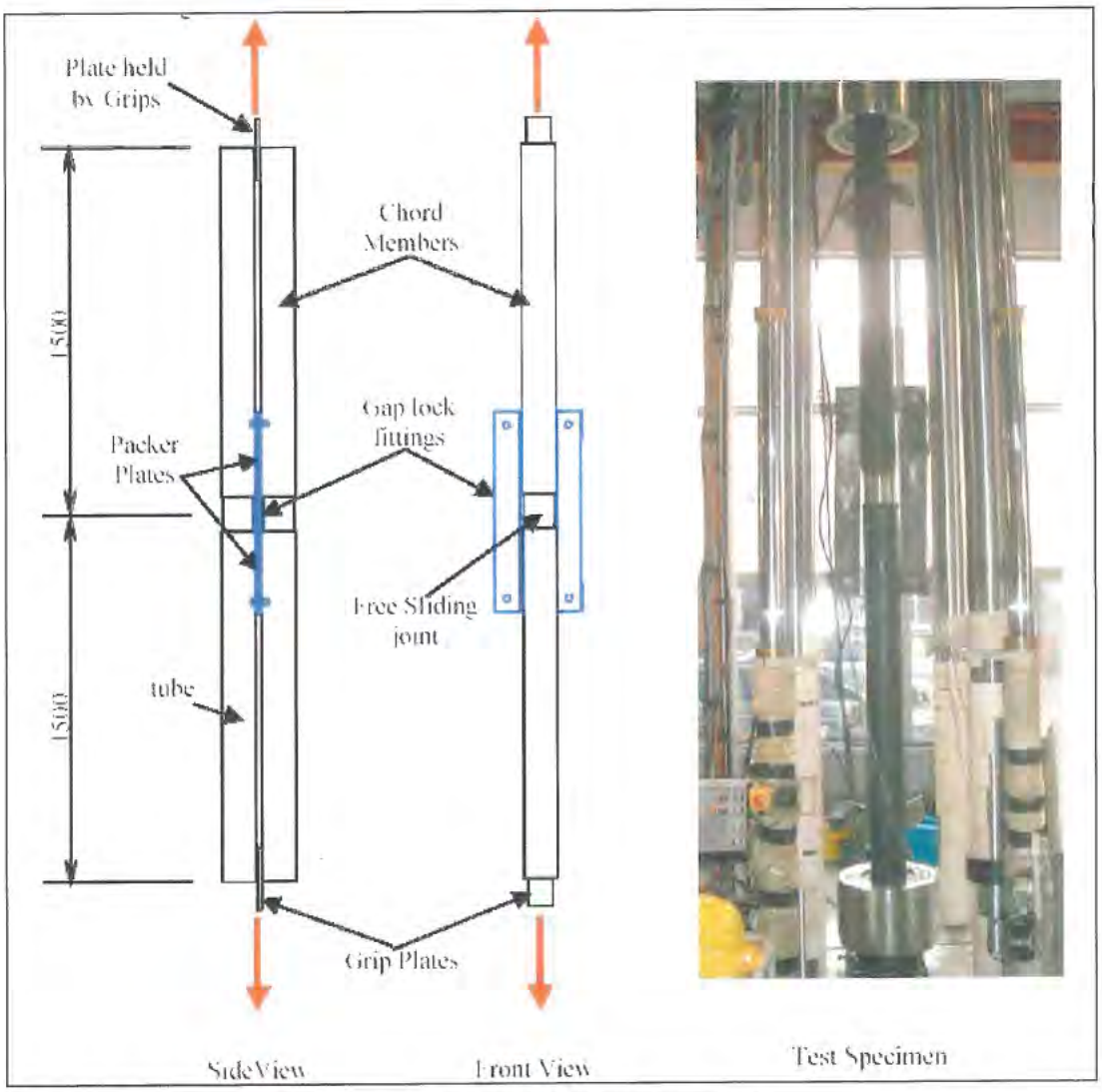

Figure 12: The test rig used for testing the gap locks (Wheeler 2004).

The width of the end plate on the gap lock was found to be either 100 mm or 110 mm from examination of the gap locks recovered from the failed structure. Gap locks with both these dimensions were included in the test programme. The nomenclature used for the plates forming the gap locks is indicated in Figure 13. Four M20 bolts were used to assemble each gap lock.

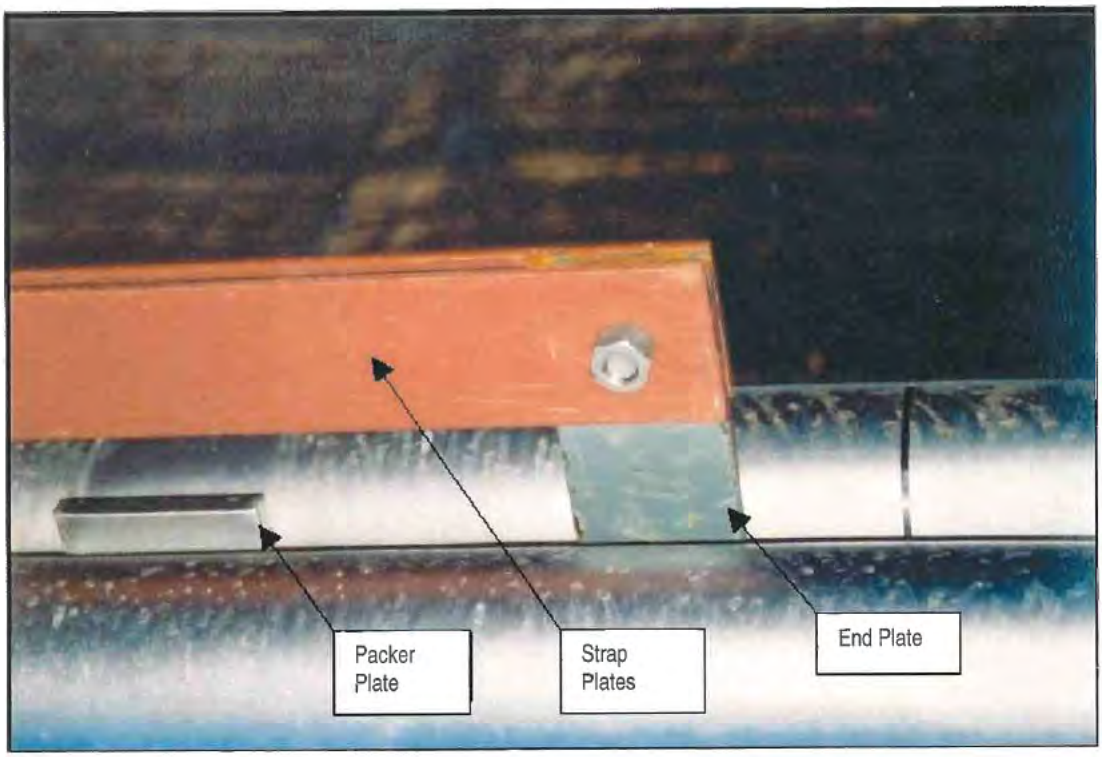

Figure 13: Part view of a gap lock together with the naming convention used for the gap lock parts.

From a functional point of view two different bolt lengths were included in the test programme (Wheeler 2004). What will be referred to as "short" bolts had the first shear plane, between the first strap plate and the end plate, located in the shank of the bolt. The second shear plane, between the second strap plate and the end plate was located at the threaded section of the bolt. The other bolt type, referred to as "long" bolts had both shear planes located in the shank section of the bolt. Figure 14 provides examples of the two bolt types described (Wheeler 2004). The blue line indicated at 28 mm coincides with the position of the second shear plane (when washers are not used). The four shorter bolts on the left fit into the short bolt category described above. The three longer bolts on the right fit into the long bolt category.

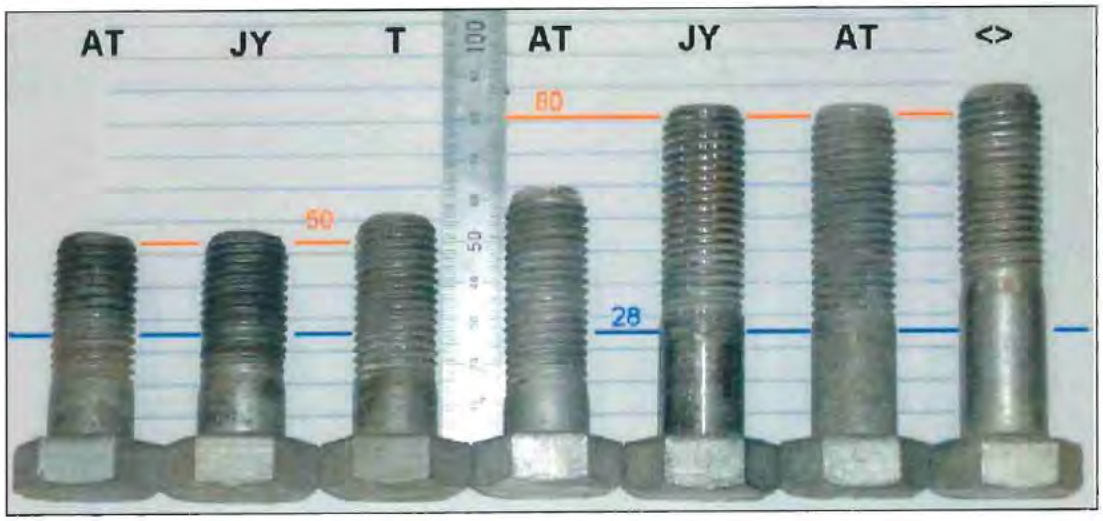

Figure 14: Examples of the bolt types used in testing (Wheeler 2004).

The geometric relationship relates to the degree of eccentricity with which the gap lock component is loaded. Two configurations were considered. The first (type A) had the bolts firmly tightened such that the top strap plates of the gap lock rest on the top of the packer plate between the lower chord members. The second configuration (type B) required the bolts to be sufficiently loose (4 mm) so that the top strap plates could drop down outside the packer plate resulting in greater preferential loading of the top plates during testing. These two configurations are indicated in Figure 15.

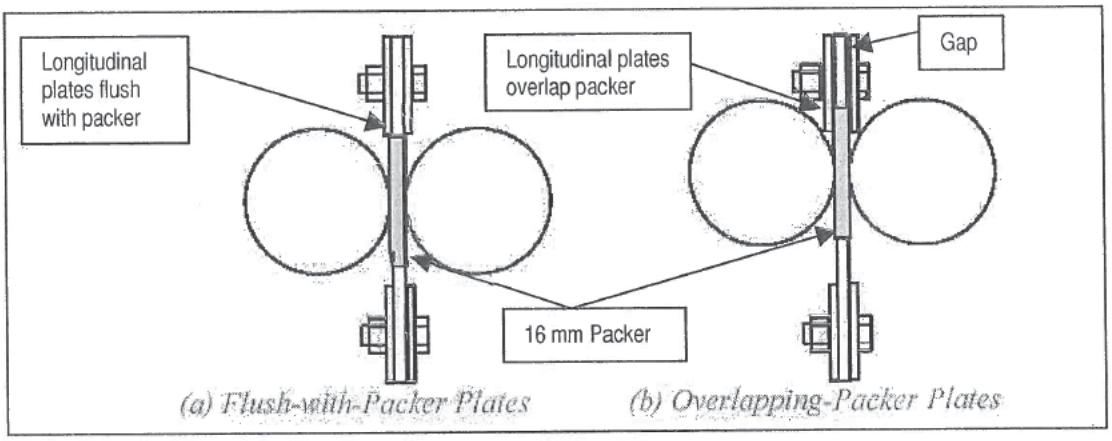

Figure 15: Two gap lock configurations tested (Wheeler 2004).

A summary of the results from the nine gap lock tests is provided in Table 2.

Table 2: Summary of test results from the gap lock testing (Wheeler 2004).

Specimen No.	Testing Order	Configuration			Results			
		End Plate Width (mm)	Bolt Type	Eccentricity	MHL*	Ultimate Load (kN)	Preferential Side (kN)**	Failure Mode
1	3	110	short	type A	58	396	230.5	bolt shear in threaded section
2	1	100	short	type A	57	362	203.9	bolt shear in threaded section
3	2	100	short	type A	60	322	195.5	bolt shear in threaded section
4	5	100	long	type B	75	390	291.4	plate edge tear out
5	4	110	short	type A	57	343	218.4	bolt shear in threaded section
6	7	100	short	type A	62	334	200.7	bolt shear in threaded section
7	8	110	short	type B	72	326	234.4	bolt shear in threaded section
8	9	100	long	type A	61	514	295.5	large deformation
9	6	110	long	type A	58	534	310.0	large deformation

* MHL refers to the load percentage carried by the two strap plates on the side of the gap lock which is preferentially loaded due to eccentricity.

** Preferential side lists the total load carried by the two strap plates that are preferentially loaded due to eccentricity.

Figure 16 provides a summary of the load versus displacement curves generated from the tests. Figure 16 and Table 2 both indicate a clear split in the results where the specimens with long bolts reaching much higher load levels before failure compared with specimens with shorter bolts. Specimen 4 appears to be an exception to this until the premature mode of failure is taken into account. This is a plate tear-out failure mode with no bolts failing in shear. This failure mode was not observed in any of the gap lock assemblies in the collapsed hangar structure.

The specimens with short bolts failed at a single shear plane in the threaded section of one of the bolts. The failed bolts were located on the preferentially loaded side of the gap lock in each instance.

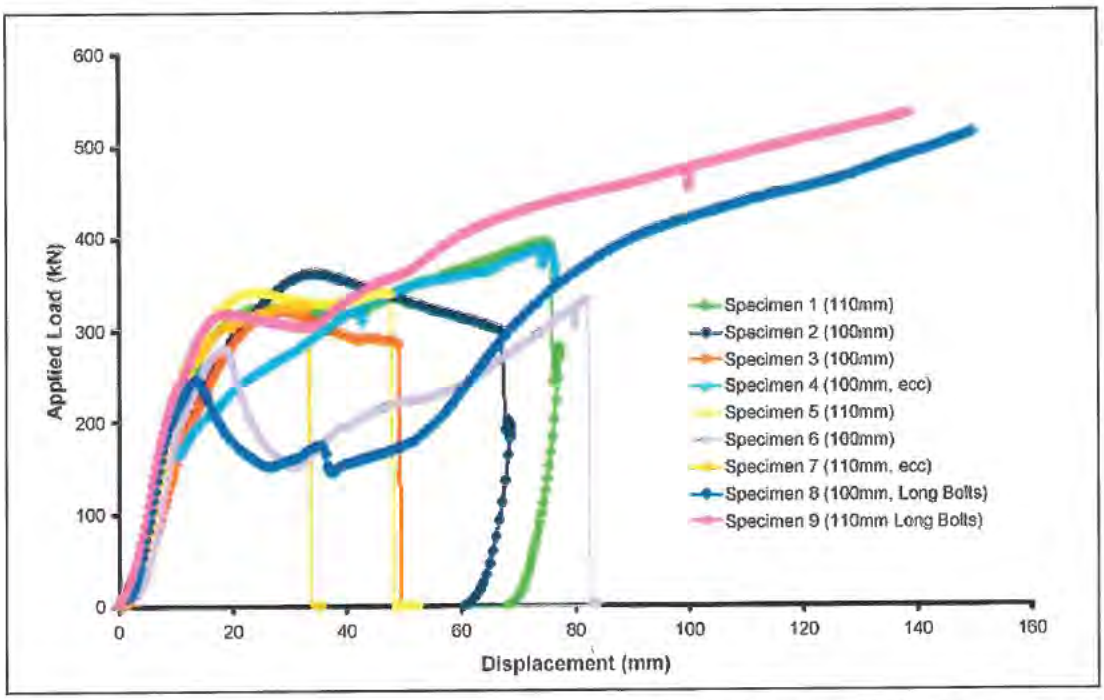

Figure 16: Total load (kN) versus cross head displacement (mm) curves for the nine gap lock specimens tested.

Figure 16 shows that most specimens exhibited an initial yield. After this yield the load dipped prior to increasing again and then failing. The magnitude of this "dip" in the load profile generally increased for the later specimens. This was because the test rig tubes adjacent to the end plate became progressively distorted as testing progressed. This occurred as the yielding of the end plate (at the initial yield point) resulted in the gap lock bearing upon the adjacent tubes. The amount of restraint provided by the adjacent tubes decreased for later tests (due to distortion of the tubes). As the end plate distorts, once the adjacent tubes provide sufficient restraint the load displacement curve trends upwards again. This effect resulted in a larger dip in the load displacement curve for later specimens.

4. Discussion

4.1 Analysis Results

The analysis results indicate that the model is adequately simulating the theoretical performance of the hangar structure. The progressive closing of the lower chord elements and the activation of the gap-lock elements seem reasonable. The calculated cable tensions at lift-off are reasonably close to the figures calculated by Strarch, considering that the analytical model makes no allowance for friction between the cable and lower chord elements.

The analysis results indicate that none of the permanent structural members were overloaded at the time of the roof collapse.

In the case of the temporary gap lock elements, the analysis indicated a load range of 350-392 kN, with full roof sheeting loads applied (based on the lower and upper bound loads, respectively). Reported analyses by others yielded gap lock loads ranging from 311 kN (as calculated by the hangar designer, Strarch International 2003b p29) to 360kN (as calculated in Arup 2003 p12).

Note that the analysis results presented here do not allow for possible differential loading between adjacent frames, wind loads on the structure, and secondary actions induced by geometrical imperfections. Such effects could cause higher forces in the gap locks than those calculated.

The analysis also excluded any allowance for "live "loads – ie personnel, tools, equipment and the like –on the basis that such loads would have been small at the time of the collapse, since very few personnel were on the roof. The relevant Australian Standard (AS 1170) specifies a live loading allowance of 0.25 kPa for roofs of this nature – ie "non-trafficable" roofs.

The application of the roof sheeting loads (0.14 kPa) increased the maximum (upper bound) gap lock load by 132 kN (ie, from 260kN to 392kN). If the normal Australian Standard live loading allowance of 0.25 kPa was also included in the analysis, the gap lock load would increase by a further 235kN, to 627 kN, well beyond the tested failure load of the gap lock component.

It should be noted that the design live load of 0.25 kPa specified by the Australian Standards (AS1170) for "non-trafficable" roofs would represent a substantial loading on Frame 6 of 2.46 kN/m - ie. approximately 250 kg/m. Over the full 95m length of the top chord of the roof truss this represents approximately 24 tonnes, and is clearly an overestimate of the actual live loading at the time of the collapse.

Given that a limited number of workers were on the roof during erection, the actual "live load" was clearly much less than the Australian code value. However additional loading could also have been applied due to wind effects, differential or concentrated local loads, and/or secondary actions due to the geometrical imperfections. Thus it is conceivable that gap lock loads at the time of the collapse could have been higher than those calculated in this report.

4.2 Testing Results

Testing carried out on gap lock assemblies (Wheeler 2004) have been described earlier in Section 3.5 of this report .

Investigation of the materials and fabrication of the hangar were also made by others (Yeomans 2004). Tensile testing of the gap lock bolts by Yeomans found that the tested bolts met their mechanical property specification (Yeomans 2004 p17). Examination of the failed gap locks indicated that the end

plates of the frame 6 and 7 gap locks had been distorted severely (Yeomans 2004 p26) in a pattern similar to that observed in the gap lock component tests described earlier in this report.

Testing of gap lock components indicated a capacity range, with short bolts, of 322-396 kN. For properly assembled gap locks (ie with bolts tightened), with long bolts, ultimate loads in excess of 500 kN were achieved.

The theoretical shear capacity of M20 grade 8.8 bolts can be determined in accordance with AS4100 (Clause 9.3.2.1). In the case of one shear plane being in the threaded section of the bolt and one in the shank a theoretical capacity of 288 kN is arrived at (excluding any capacity reduction factor). For both shear planes through the shank section of the bolt a capacity of 323 kN results.

Inspection of Table 2 (preferential load column) indicates that for the "short" bolt configuration none of the bolts achieved this capacity prior to failure. The "long" bolt tests came close to the nominal capacity but either failed through a different mode (tear out of end plate) or were stopped prior to failure.

The tests also indicated that the failure of all bolts was preceded by lateral deflection and plastic deformation of the end plates (refer Appendix C). This suggests that the end plates have reached their structural capacity before the bolts.

This observation is explainable by theory. It can in fact be shown by simple manual calculations that the end plates reach their theoretical bending capacity at a stage that the bolts are loaded at around half their theoretical capacity.

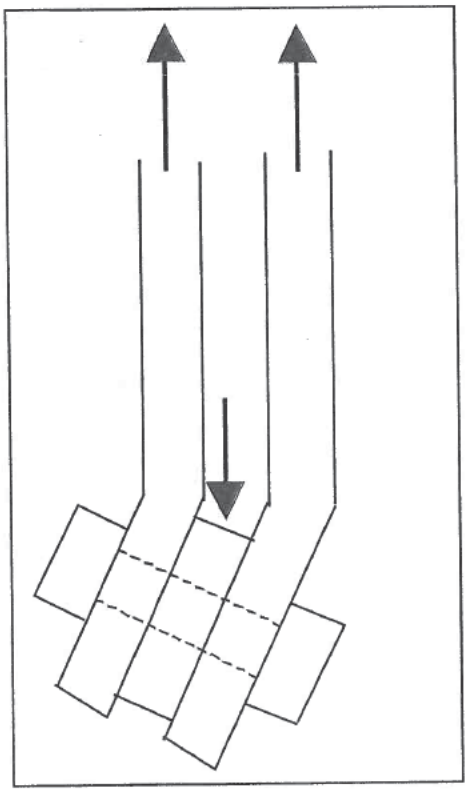

Figure 17: Diagram of forces applied to distorted gap lock (plan view).

The mechanism of failure after lateral distortion of the end plates is depicted in Figure 17. The lateral distortion of end plates leads to a prying effect on the bolted joint and induces a complex loading state in the bolt, beyond the design shear loads. The interaction of combined shear and tension leads to a reduction in the theoretical shear capacity of the bolts. This is supported by the test results, which show gap lock failure loads less than the theoretical failure capacities of the bolts.

In summary, the gap lock tests indicate that the likely sequence of failure of the critical gap lock is as follows:

- The gap lock end plate starts to yield and distort under increasing loads.
- The end plate distortion results in a complex stress state (involving combined shear, bending and tension) in the bolts on the preferentially loaded side of the gap lock.
- One of these bolts fails in a single shear plane through the threaded section of the bolt.
- The failed bolt is pulled out of the distorted plates, before a failure at the second shear plane can occur.
- The gap lock comes apart.

4.3 Comparison of Analysis and Testing

The results from analysis indicate that the likely load applied to the critical gap lock component in Frame 6 of the structure at the time of failure was in the range 350-392 kN. However, results from testing show that a gap lock component, assembled with short bolts, has a failure capacity in the range of 322-396 kN with a mean value of 347kN which is less than the likely range of loads in the gap lock.

Given the evidence (Yeomans 2004) that a significant proportion of the gap locks had been found to have the short bolts, it is considered reasonable to use the "short bolts" test results as a measure of the available gap lock capacity at the time of collapse.

On this basis, the collapse of the structure is consistent with the findings of this report which indicate that a critical gap lock in the structure could be at or close to failure under the level of loading applied at the time of collapse.

4.4 Commentary on Gap Lock Safety Factor

The comparison presented in Section 4.3 indicates a safety factor (ie, strength divided by load) of near one. It should be noted that this is significantly less than what is commonly achieved in design practice. For a structure subjected to self-weight and dead loads only the design safety factor is commonly in excess of two.

One of the key characteristics of this hangar roof structure is that the integrity of the whole structure depends on the strength of individual gap locks. This characteristic is often referred to as "lack of redundancy" of the structure. For structures of this type, a higher safety factor is often adopted in practice.

Given the observed failure mode of the gap lock, an increased safety factor could have been achieved by using one or a combination of the following measures:

- Increased number of bolts in the critical gap locks (to decrease loads imposed on each bolt)
- Larger diameter bolts for the critical gap locks (to decrease stresses imposed on the bolts)
- Larger and/or thicker end plates in the critical gap locks (to stop the undesirable lateral distortion and the ensuing detrimental "prying" action on the bolts)

5. Conclusions

Based on the analytical and experimental work described in this report, it is concluded that the likely cause of the hangar collapse is as follows:

- The loading present at the time of collapse exceeded the capacity of the bolted connections of a single gap lock.
- This led to the failure of that gap lock and the frame of which it formed a part.
- Once the first frame started to collapse, differential loading of adjacent frames resulted in their gap lock elements being loaded beyond their capacity and caused a domino effect with all frames progressively failing.

The topology of the failed hangar structure documented in Appendix A is consistent with the scenario outlined above.

6. References

- Arup 2003 *Capital Airport Group, Special Purpose Aircraft Facility Fairbairn, Hangar Roof Failure Investigation* Arup, Sydney.
- Strarch International 2003a *Strarch International Limited, Canberra SPAF, Investigation Report No. 1, Hangar Collapse, Factual Observations* Strarch International Ltd., Sydney.
- Strarch International 2003b *Strarch International Limited, Canberra SPAF, Investigation Report No. 2, Hangar Collapse, An Investigation of the Hangar at Collapse* Strarch International Ltd., Sydney.
- Strarch International 2003c *Structural Engineering Calculations for Erected Hangar, Volume 3/4* Strarch International Ltd., Sydney.
- Wheeler A 2004 *Testing of gap lock fittings - Strarch hanger collapse causation investigation* Centre for Construction Technology and Research, University of Western Sydney, Sydney.
- Yeomans S 2004 *Investigation of Materials and fabrication from SPAF Hangar Collapse, Fairbairn ACT* Unisearch Ltd Sydney.

Appendix A: Photos of Failed Structure

Figure A1: Global View of the failed structure. Note 3.5 bays have had roof sheeting applied.

Figure A2: Failed gap lock at SF6

Figure A3: Failed gap lock plate on SF4.

Figure A4: SF8, failed gap lock plate and buckled top chord.

Figure A5: Failed gap lock plate on SF5.

Figure A6: View from above, over central section of SF7. Note the buckled top chord.

Appendix B: Model Input Data

Table B1: Real constant properties used in the ANSYS model. Length units are metres.

RC Set 1	AREA (m^2)	Izz (m^4)	Iyy (m^4)	Tkz (m)	Tky (m)	Theta	Istrn	Ixx (m^4)
1	6.60E-03	3.92E-05	3.92E-05	0.2	0.2	0	0	6.45E-05
2	4.24E-03	9.68E-06	3.05E-05	0.1397	0.1397	0	0	1.94E-05
3	5.72E-03	1.35E-05	3.58E-05	0.125	0.125	0	0	2.02E-05
4	0.1124	6.85E-05	5.72E-05	0.3	0.3	0	0	5.33E-07
5	6.66E-03	1.77E-05	5.28E-05	0.2	0.2	0	0	3.25E-07
6	1	1000	1000	1	1	0	0	1000
7	1.25E-03	1.92E-06	1.92E-06	0.1143	0.1143	0	0	3.84E-06
8	1.85E-03	2.75E-06	2.75E-06	0.114	0.114	0	0	5.49E-06
9	1.88E-03	4.52E-06	4.52E-06	0.125	0.125	0	0	7.25E-06
10	1.48E-03	2.23E-06	2.23E-06	0.1	0.1	0	0	3.63E-06
11	1.67E-03	0	0	0	0	0		0
12	4.53E-03	2.80E-05	2.80E-05	0.2	0.2	0	0	4.48E-05
22	2.28E-03	5.14E-06	5.14E-06	0.1397	0.1397	0	0	1.03E-05
23	0	0	1	0	0	0	0	0
24	3.20E-03	0	0	0	0	0	0	0
25	0.2	0	0	0	0	0	0	0
26	4.24E-03	0	0	0	0	0	4.90E-02	0
27	4.24E-03	0	0	0	0	0	5.20E-02	0
28	4.24E-03	0	0	0	0	0	5.40E-02	0
29	4.24E-03	0	0	0	0	0	5.90E-02	0
30	4.24E-03	0	0	0	0	0	4.40E-02	0
31	4.24E-03	0	0	0	0	0	6.50E-02	0

Table B2: Range of applicability of various real constant sets.

RC1 = 200 x 200 x 9 SHS 350, Generally top chord
RC2 = 2 x 139.7 x 5 CHS 250, not used, bottom chord flexible section
RC3 = 2 x 125 x 6 SHS 350, bottom chord fixed section
RC4 = plate section, extension of bottom chord to jacking plate
RC5 = 200UC52 300, outside members on side leg.
RC6 = plate section, bottom of side legs at supports
RC7 = 114.3 x 3.6 CHS 350, web members at centre of flexible section
RC8 = 114.3 x 5.4 CHS 250, web members at sides of flexible section
RC9 = 125 x 125 x 6 SHS 350, web members, rigid section
RC10 = 100 x 100 x 4 SHS 350
RC11 = Cable
RC12 = Not Used
RC22 = Not Used
RC23 = Not Used
RC24 = Gap lock Elements, tension only
RC25 = Scaffold supports, Compression only
RC26 = Bottom chord flexible section, Compression only
RC27 = Bottom chord flexible section, compression only
RC28 = Bottom chord flexible section, compression only
RC29 = Bottom chord flexible section, compression only
RC30 = Bottom chord flexible section, compression only
RC31 = Bottom chord flexible section, compression only

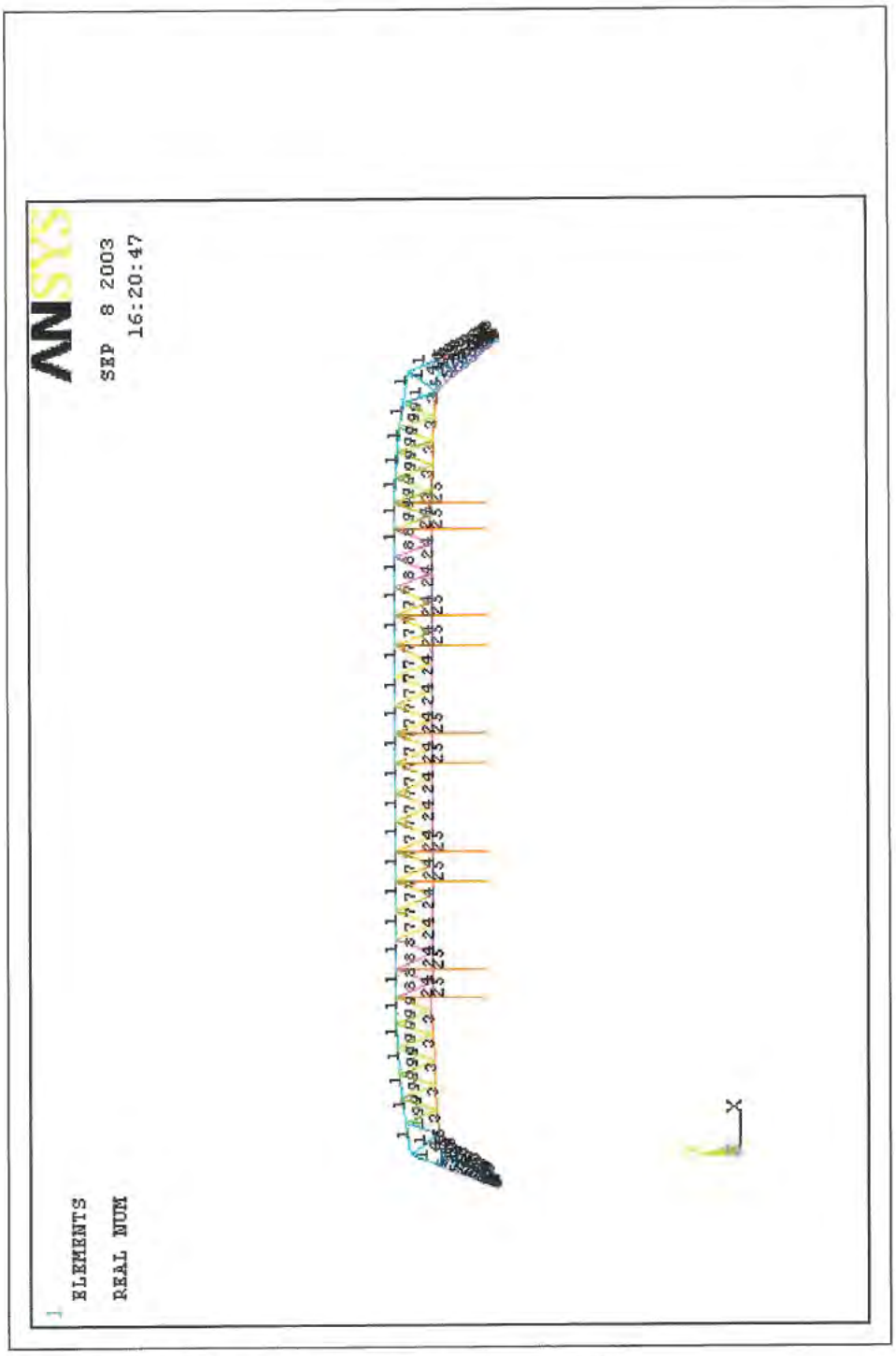

Figure B1: Application of real constant sets to the model.

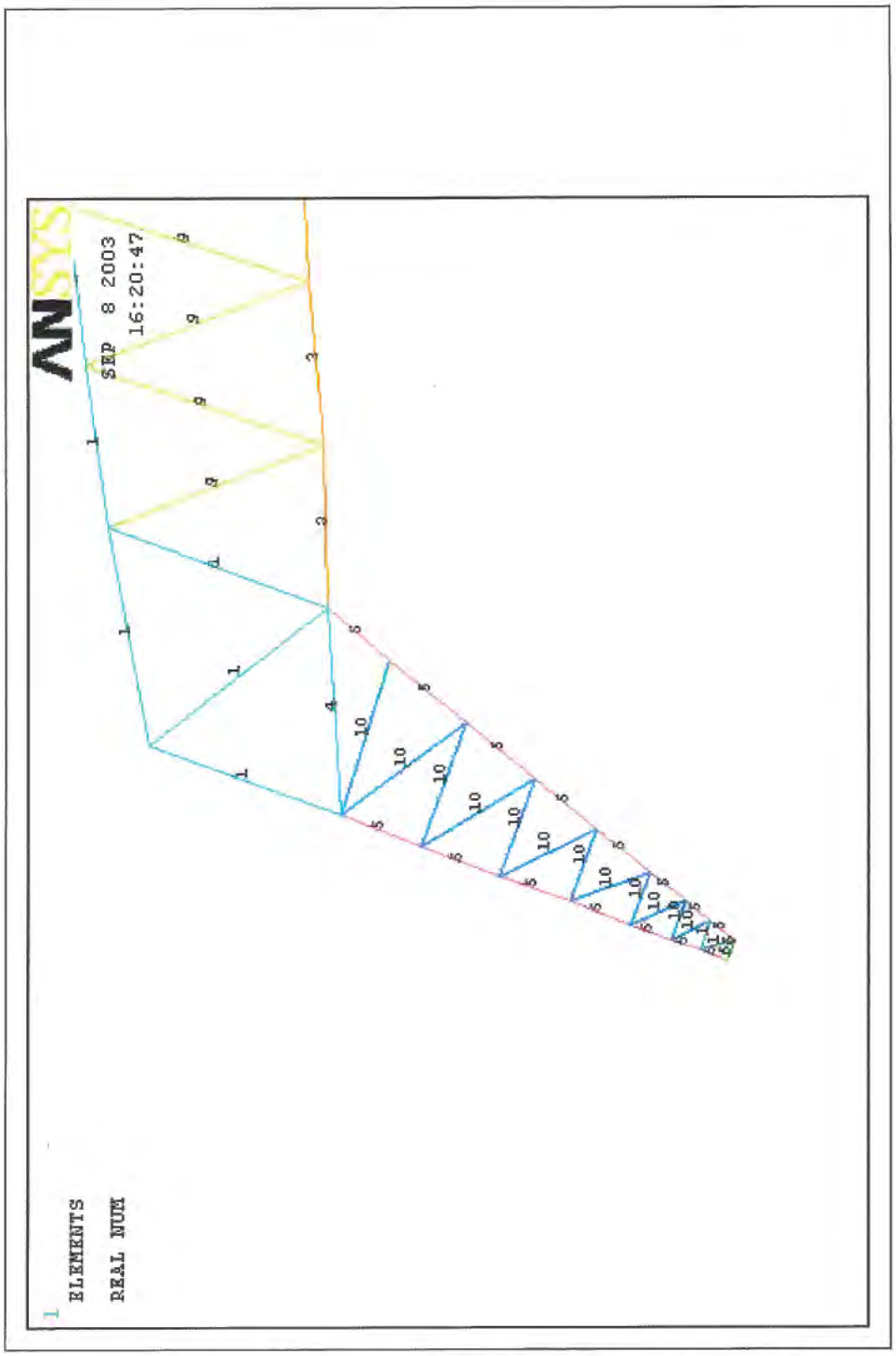

Figure B2: Application of real constants, zoomed in to left hand side leg of structure for clarity.

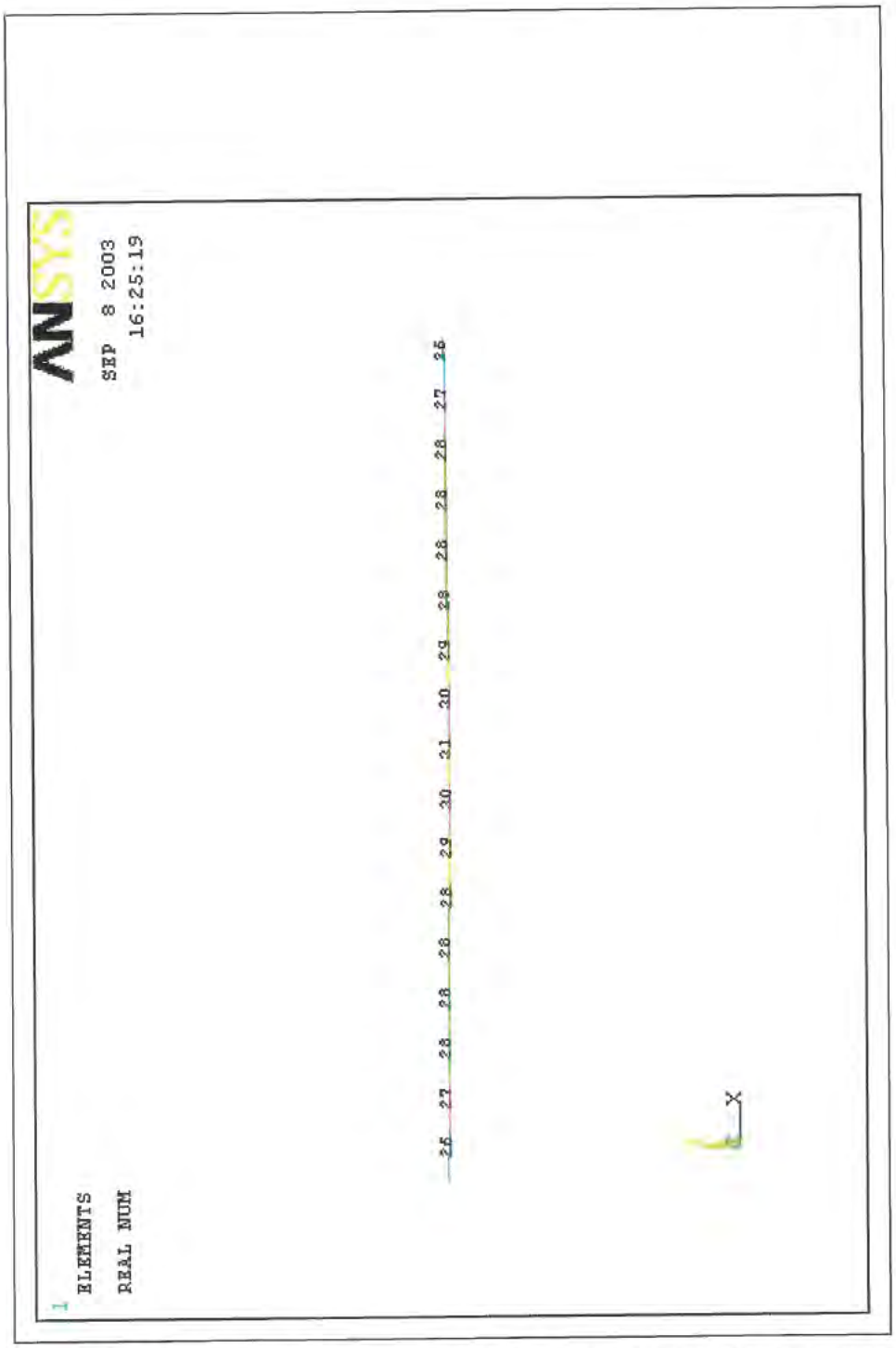

Figure B3: Application of real constants to the compression only elements in the flexible bottom chord section. Different properties were used as the gap between adjacent sections varied along the length.

Appendix C: UWS Gap Lock Component Testing Report

CENTRE FOR CONSTRUCTION TECHNOLOGY AND RESEARCH
College of Science, Technology and Environment
Locked Bag 1797, Penrith South DC, NSW 1797

University of Western Sydney
ABN 53 014 069 881

Test Report
CCTR-TR-04-03

June 2004

Testing of Gap Lock Fittings – Strarch Hanger Collapse Causation Investigation

Summary

Nine tensile tests have been carried out on gap lock fittings taken from the site of a Strarch hanger. The specimens were supplied by ACT WorkCover. The tests were conducted using a testing assemblage designed to closely simulate the site conditions. Variables in the test program included the location of the shear planes within the bolt (shank or thread), end plate width and eccentricity of the fitting relative to the line of force.

The dominant failure mode observed was fracture of the bolts through the thread. The relationships between the applied load and cross-head movement, and the measured strains in the strap plates, are presented along with test photographs.

1 Introduction

1.1 Client

ACT Workcover
Level 4, Eclipse House,
197 London Circuit
CANBERRA CITY ACT 2601

PO Box 224
CIVIC SQUARE ACT 2608

1.2 Purpose

On the 7th of May 2003 an aircraft hanger being constructed in Canberra using the Strarch Frame System collapsed. The test program detailed herein was carried out to ascertain the strength of the gap-lock fittings that are believed to have contributed to the collapse of the structure.

Connell Mott Macdonald has conducted a various analyses into the possible cause of collapse of the Strarch aircraft hanger on behalf of Work Cover ACT. A number of other failure reports have also been prepared by other organisations. Reports prepared on behalf of Strarch International have concluded that a contributing factor of the collapse was the premature failure of one or more of the gap-lock fittings used as temporary members during the erection process.

The analysis conducted to date on behalf of Work Cover ACT has suggested that forces in the gap lock fitting at failure were considerably less than the load that is assumed to cause failure of the fitting. Furthermore, it has been suggested that eccentric loading may result is a premature failure of the fitting. In order to determine the force to fail the fitting, and investigate the effect of eccentric loading a program of testing be carried out. Strarch international has already had testing carried out on their behalf by the University of Sydney but further checking is required.

1.3 Specimens

The test program detailed in this report involved the testing of nine gap lock specimens; the variables included the bolt length and configuration, the applied eccentricity and the end plate width. Each specimen comprised two end plates and four strap plates. These plates were connected using four M20 bolts as shown in Figure 1. All nine specimens tested where supplied by ACT WorkCover with individual plates labeled upon arrival.

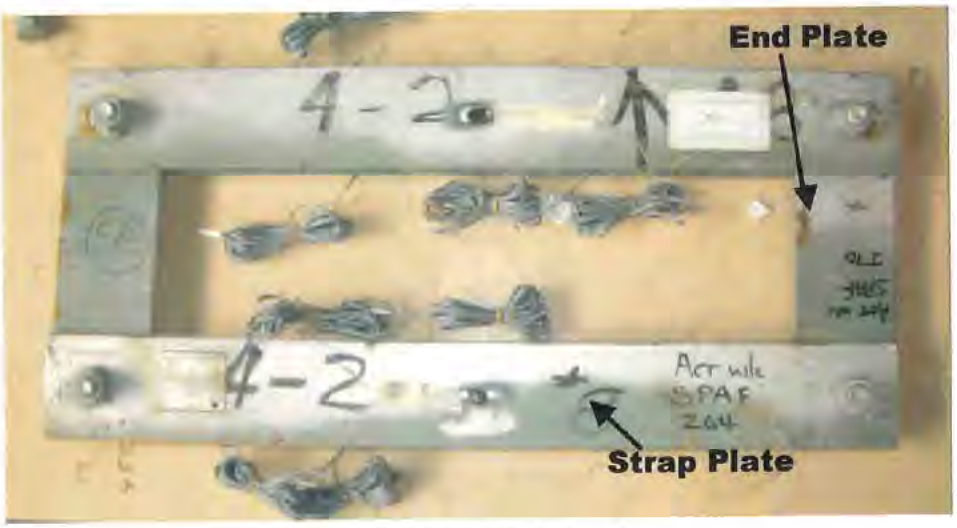

Figure 1 – Gap-Lock Specimen

The measured dimensions of the strap and end plates for each specimen are presented in Table 1. All specimens appeared to be in good order, with the plates undamaged except for some minor surface damage, these blemishes were probably the result of transportation.

Table 1 – Specimen Plates Details

Specimen #	Strap Plates			End Plates		
	Width (mm)	Thickness (mm)	Length (mm)	Width (mm)	Thickness (mm)	Length (mm)
1	100	8.2	815	110	12.3	360
2	100	7.9	815	100	12.1	360
3	100	7.8	817	100	12.0	360
4	100	8.1	815	100	12.0	360
5	100	8.2	815	100	12.3	360
6	100	8.1	815	100	12.1	360
7	100	8.2	815	110	12.3	360
8	100	8.2	815	100	12.3	360
9	100	8.1	815	110	12.2	360

1.3.1 Bolts

In addition to the bolts supplied in the assemblies, ACT WorkCover supplied numerous additional bolts to be used in the test program. Upon inspection of these additional bolts it was established that there were four different bolt manufacturers and five different bolt lengths.

All bolts were M20 and marked with three radial lines and an 8.8 indicating structural grade 8.8 bolts. The various lengths of bolts are shown in Figure 1. As a reference the 50 mm and 80 mm lengths are shown in the figure. Also presented is the location of the second shear plane assuming a strap plate thickness of 12 mm and an end-plate thickness of 16 mm. The manufacturers markings found on the bolt heads are also presented above each of the bolts.

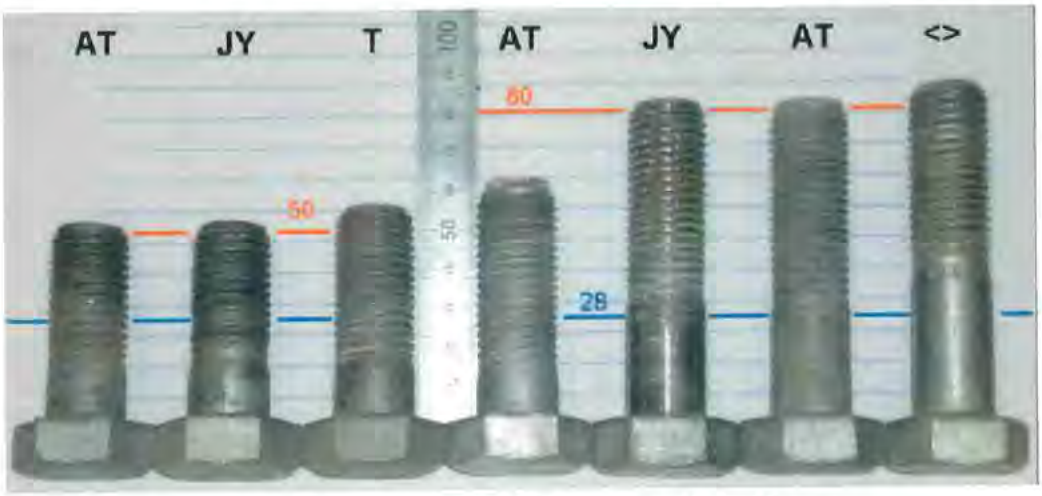

Figure 2 – Varying Bolt lengths and Markings

For consistency, the type and length of all the bolts used in each specimen were kept constant. However, they varied between tests. The bolt length and markings for each test are detailed in Table 2 along with the orientation of the bolt head, noting that "heads front" indicates that the heads were on the same side of the testing rig as the controller. The table also indicates if a washer was utilised between the nut and strap plates.

Table 2 - Specimen Bolt Details

Specimen #	Bolt Type and Orientation				
	Marking	Washers	Length	Orientation Top	Orientation Bottom
1	JY	No	50	Heads Rear	Heads Rear
2	AT	No	50	Heads Rear	Heads Front
3	AT	No	50	Heads Front	Heads Front
4	AT	Yes	85	Heads Rear	Heads Rear
5	AT	No	60	Heads Front	Heads Front
6	AT	Yes	60	Heads Rear	Heads Rear
7	AT	Yes	60	Heads Front	Heads Front
8	JY	Yes	85	Heads Front	Heads Front
9	JY	Yes	85	Heads Rear	Heads Rear

1.4 Location

All testing was carried out in the CCTR Structures Laboratory located at:

Building XC
University of Western Sydney
Second Avenue
Kingswood NSW 2747

1.5 Time and date

The tests were performed on

Specimen 1	-	27th, May 2004.	Observed by Kourosh Kayvani
Specimen 2	-	26th, May 2004.	Observed by Wayne Spencer
Specimen 3	-	26th, May 2004.	
Specimen 4	-	28th, May 2004.	
Specimen 5	-	28th, May 2004.	
Specimen 6	-	11th, June 2004.	
Specimen 7	-	15th, June 2004.	
Specimen 8	-	15th, June 2004.	
Specimen 9	-	31st, May 2004.	Observed by Kourosh Kayvani

1.6 Personnel

Prof. Mark Patrick
Director
Centre for Construction Technology and Research

Dr Andrew Wheeler
Senior Research Fellow
Centre for Construction Technology and Research

Michael Greentree
Technical Officer
Centre for Construction Technology and Research

Murray Bolden
Technical Assistant
Centre for Construction Technology and Research

2 Test Setup

2.1 Testing system

All the specimens were tested in the Instron 8504 Testing Frame utilising 500 kN hydraulic grips. A purpose-built test assembly was supplied by ACT Workcover and consisted of two portions of the bottom chord, each approximately 1500 mm long. The inner sleeve and the packer plates were identical to those detailed for the structure. The test assembly was held in the testing frame using 16 mm Bisalloy endplates, 100 mm wide, using the hydraulic grips. The length of the test assembly was selected to minimise restraint effects on the gap-locks fittings. Sketches of the testing arrangement, along with a picture of a specimen in the test rig are shown in Figure 3.

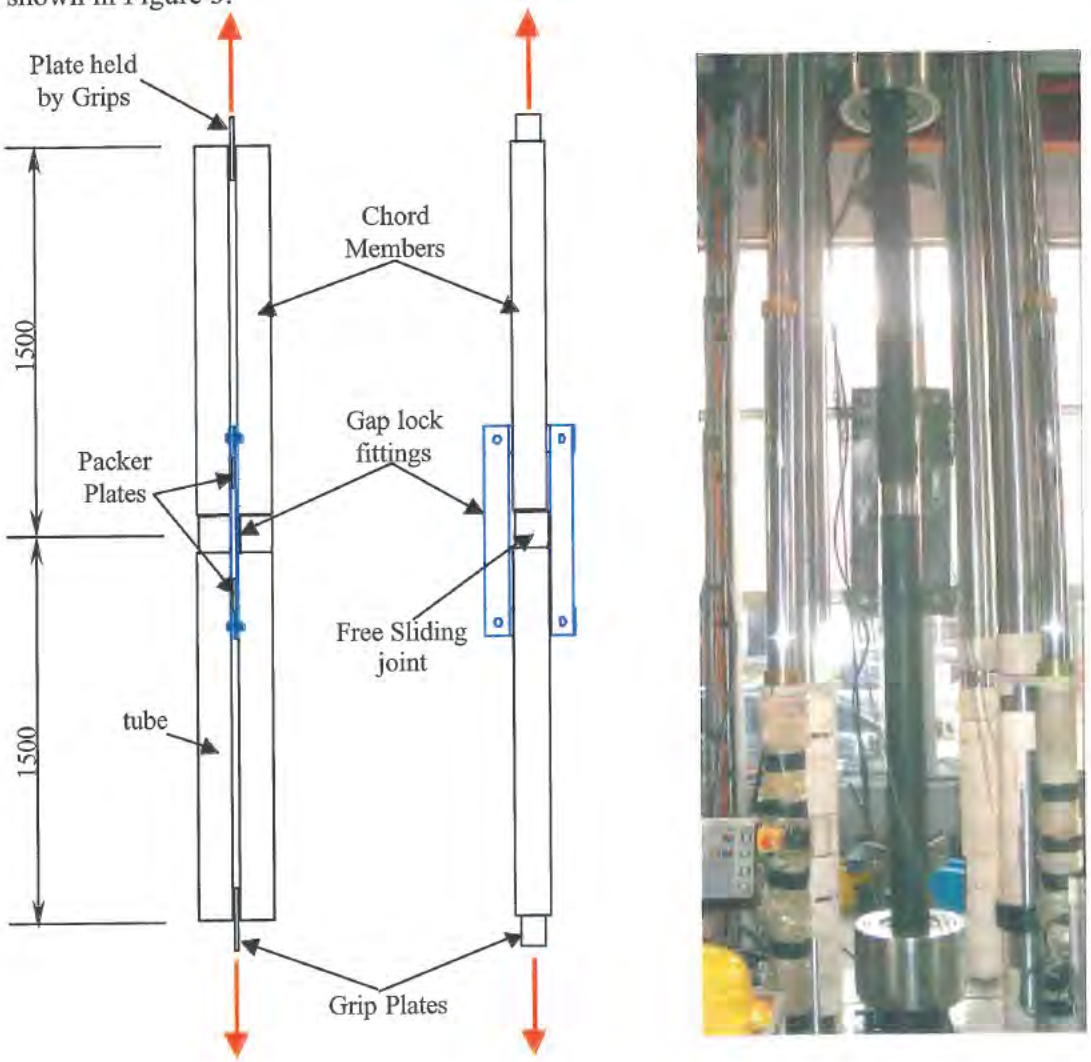

Figure 3 – Testing Arrangement and Specimen in Testing Frame

The test rig comprised of two tubular section connected together by welding of two 16 mm plate between the sections. The 16 mm plate adjacent to the gap-lock fitting is referred to as the packer plate consisted of a 150 x 150 x 16 mm plate, grade 300, with full length fillet

welds on both faces and on both tubes, fillet welds were also run on the top and bottom faces. The tensile loads applied to the gap-lock fitting are transferred through bearing of the endplates on these packer plates. The grip plates comprised of 16 mm Bisalloy plate and were designed to transfer load from the hydraulic grips to the chord members.

2.2 Loads

The applied loads were measured using an Instron 1000 kN tension/compression load cell with a current NATA Grade A approved calibration.

2.3 Movements

2.3.1 Cross-Head Movements

The crosshead movements where measured using the Instron LVDT mounted within the actuator. This LVDT has been calibrated using a NATA-approved, calibrated Digimeter.

2.3.2 Lateral Movements

The lateral deflections of the gap-lock fittings relative to the chord member were measured for the last six specimens tested, viz. specimens 4 to 9. The deflections were measured using Sakae linear potentiometers (LP's) with a 100 mm stroke that were calibrated using a NATA-approved calibrated Digimeter.

The location of a linear potentiometer is shown in Figure 4. The lateral deformation of the end plate adjacent to the bottom packer plate on the left side of the connection was measured. The LP was mounted off the chord member using a magnetic base.

Figure 4 – Lateral Linear Potentiometer

2.4 Strains

For each specimen the longitudinal strains of the strap plates were measured using a pair of strain gauges on each plate. These gauges were located in the middle of each plate on opposing faces. In total eight (8) strain gauges were used for each specimen and were all taken form the same batch and therefore had a constant gauge factor.

2.5 Data acquisition

Data acquisition was carried out using the Solartron Isolated Measuring Pods linked to the IDAS software. For all channels the raw voltage and scaled results were recorded. These results included the loads, crosshead movement, lateral displacement and strains on each face of the strap plates. The data was recorded at 3-second intervals for the duration of each test.

3 Test Procedure

The specimens were tested in two configurations, as shown in Figure 5. The configuration and bolt length for each test specimen are given in Table 3.

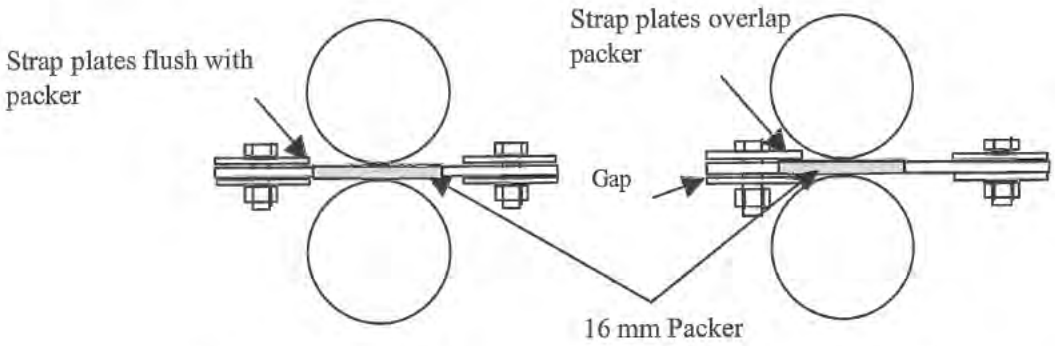

(a) Flush-with-Packer Plates *(b) Overlapping-Packer Plates*

Figure 5 – Test Configurations

The first configuration, Type A, shown in Figure 5(a) modelled the gap-lock fittings with the strap plates held flush with the end plate. The longitudinal plates on one side of the specimen beared against the packer as shown in Figure 5(a).

The second configuration, Type B, shown in Figure 5(b) modelled the gap-lock fittings with the bolts loose, allowing the strap plates to overlap both sides of the packer plate. To ensure a consistent gap, a 16 mm plate was placed between the longitudinal plates in the vicinity of the bolts, the bolts were then tightened and the 16 mm plate removed.

In both test configurations the more heavily loaded (MHL) side of the specimen refers to the side of the gap-lock fitting that carries a major part of the applied load. This corresponds to the strap plates are closest to the packer plate. In the test configurations tested herein, the MHL side is always the left side when looking from the front of the test frame.

Table 3 – Test Configuration Details

Specimen #	Configuration	End plate Width (mm)	Bolt Length (mm)
1	Type A	110	50
2	Type A	100	50
3	Type A	100	50
4	Type B	100	85
5	Type A	110	60
6	Type A	100	60
7	Type B	110	60
8	Type A	100	85
9	Type A	110	85

The loading of all specimens was carried out using displacement control with a constant crosshead movement of 0.11 mm/sec (6.5 mm/min).

4 Test Results

For each test the following three relationships are presented:

- load versus crosshead movement;
- axial strain in each strap plate versus load; and
- ratio of average strain on each side of the specimen versus applied load.

The axial strain in each strap plates was determined by averaging the strains measured on opposite faces of each plate, eliminating any bending strains. The ratio of the average strain was determined by averaging the axial strains on each side of the specimen, and then determining the relative percentage of loading carried by the MHL side of the gap-lock fitting which is defined as the side where the strap plates are closest to the packer plate. It was assumed that the strap plates had the same cross-sectional area and were from the same steel.

In all the tests, significant lateral deflections of the end plate were observed. Typical lateral deflection curves for the last six tests are shown in Figure 6. The figure demonstrates that the lateral deflection was relatively small (less than 5mm) until the end plate began to yield.

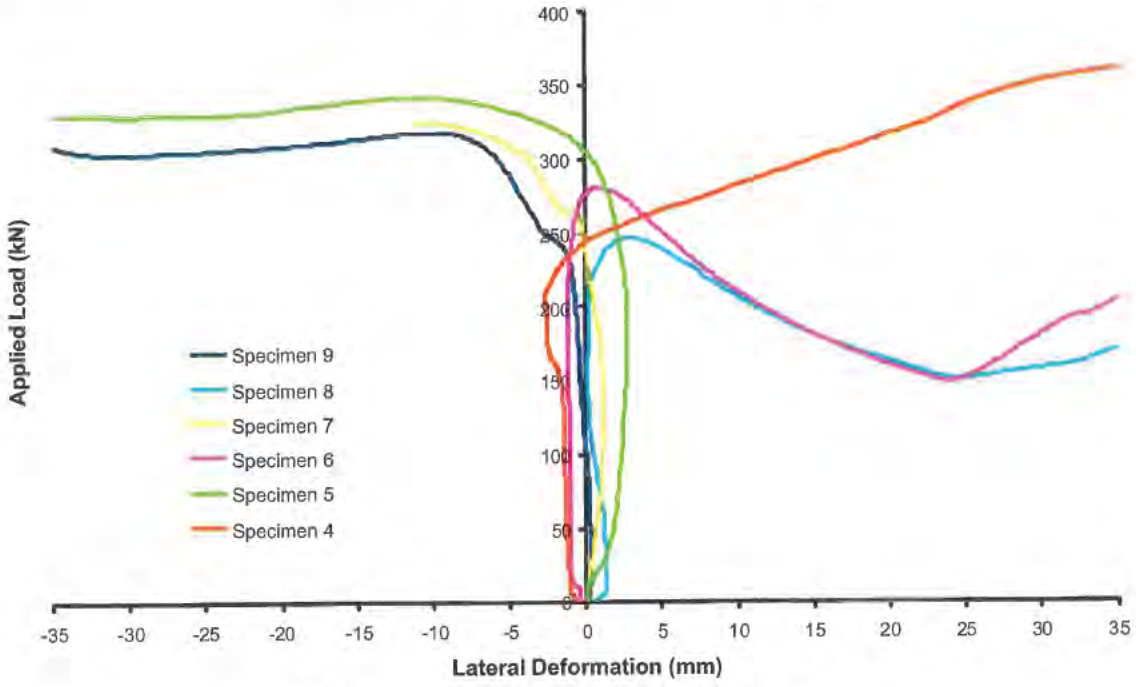

Figure 6 – Typical Lateral Displacements

The significant lateral deflections as shown in Figure 6 were observed in all the tests. In addition to this lateral deflection the end plates were also deformed significantly in the direction of the applied load as shown in Figure 7(b). Also demonstrated in the figure is that this plastic deformation resulted in the end plates twisting out of plane. This twisting action of the end plate resulted in some bending in the strap plates. This bending is shown in Figure 7(c), with a straight line superimposed to highlight the bending of the strap plates. Photographs of all the end plates when removed from the test specimen showing the deformations are found in Appendix A.

(a) Bearing of End Plate

(b) Typical Deflections of the End Plates

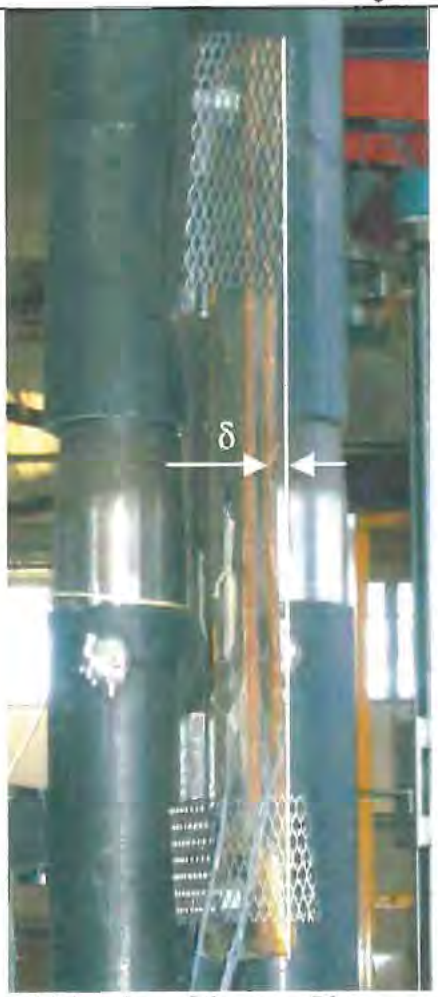

(c) bowing of the strap Plates

Figure 7 – Seating and Rotations of End Plates

It was also noted that during the manufacturing process, some weld was placed on the contact surface of the packer/end-plate interface. This weld material preventing an ideal bearing surface to form, and contributes to eccentric loading and thus twisting. Furthermore, it was noted that for most specimens the inside edge of the end plate that bears on the packer plate was not square (see Figure 7(a)) thus increasing the difficulty to obtain an ideal bearing surface.

As detailed latter during the sixth test significant deformations were imposed on the chord members, as a result the free sliding joint could no longer be closed. To complete the test series 400 mm of chord was removed from the test frame and an identical packer plate placed and the tests completed.

During the tests as the endplate twisted it beared on the chord members, as the load increased some plastic deformations were imposed on the chords, with the plastic deformations increasing as further tests were carried out. This effect is demonstrated in the last three tests, where one half of the gap-lock fitting is partially restrained by an undeformed chord member, and the other member less-restrained due to deformations in the chord. In these tests the loads increase to the yield load and then significantly drop prior to failing at loads similar to previous specimens.

4.1 Individual Tests

4.1.1 Test #1 - Specimen 2

Specimen 2 had an end-plate width of 100 mm, tested using configuration Type A. In this test only one peak load prior to failure of the gap-lock fitting was observed. This peak load of 361 kN occurred at a crosshead displacement of 34 mm. A further 33 mm of displacement was observed prior to failure at 297 kN. The failure mode for specimen 2 was a shear failure of the top left-hand bolt through one shear plane located in the threaded section of the bolt. After the failure of the bolt one shear plain remained intact, thus some load was still carried after the initial failure of the bolt.

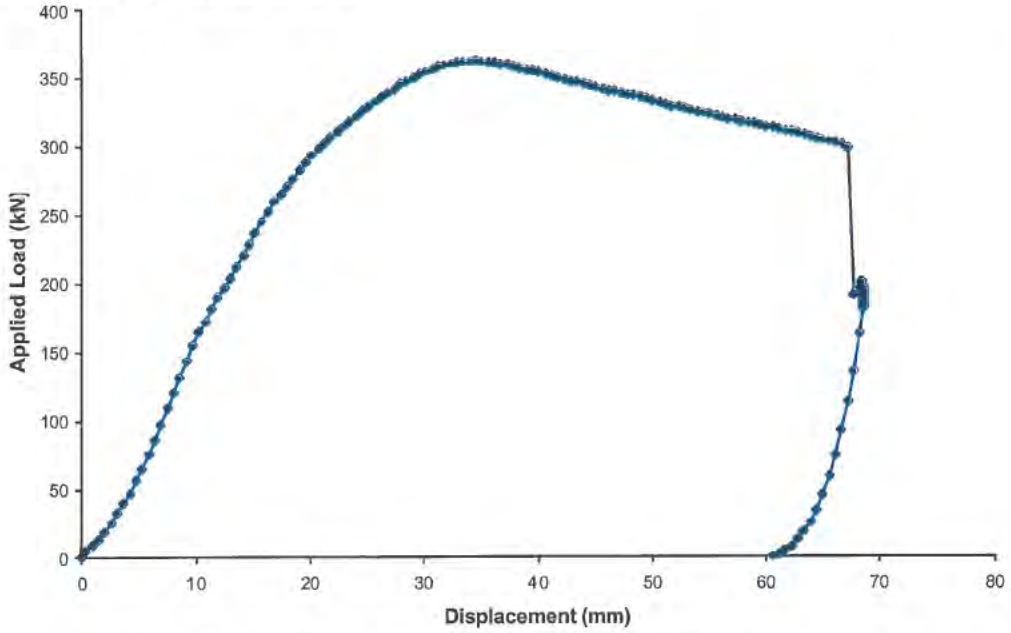

Figure 8 - Specimen 2 - Load vs Cross-Head Displacement Curve

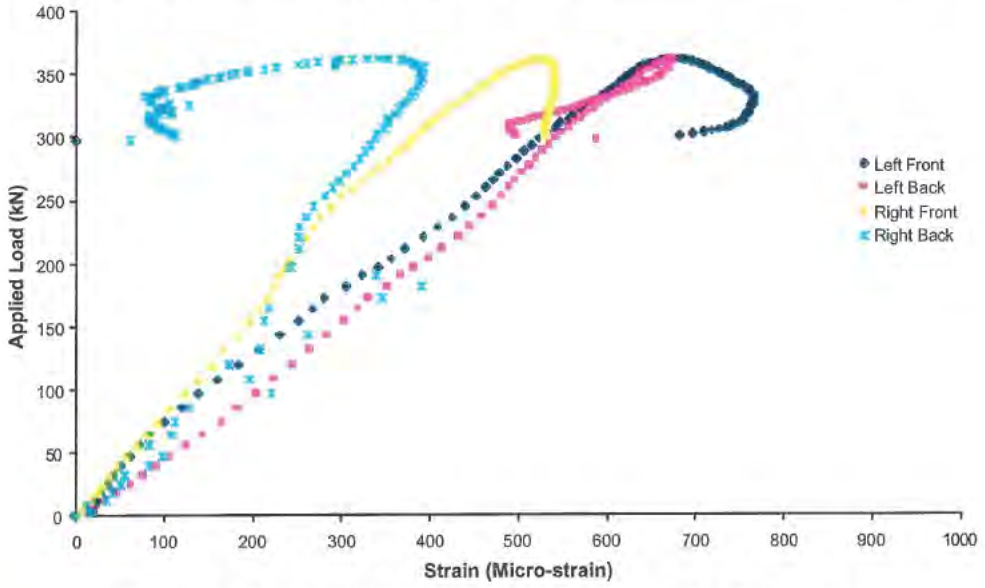

Figure 9 - Specimen 2 - Load-Strain Curves for Strap Plates

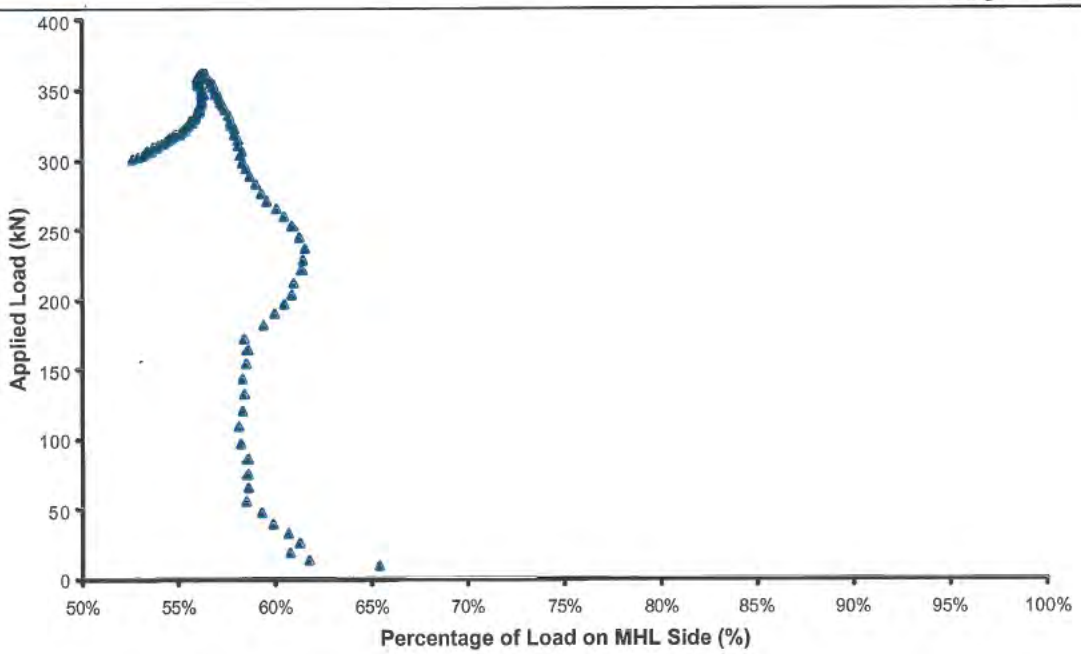

Figure 10 – Proportion of Load carried on MHL Side

The mode of failure is clearly visible in Figure 11(a) with the front strap plate separating from the end plate as a result of shear failure of the bolt. The head-side of the bolt and rear strap plate remained in place and continued to carry over 200 kN. The lateral movement of the end plate was towards the rear of the test assembly as can be seen in Figure 11(b)

(a) Bolt Shear *(b) Lateral Movement*

Figure 11 – Failure Mode of Specimen 2

4.1.2 Test #2 - Specimen 3

Tested using the Type A configuration, specimen 3 with an end-plate width of 100 mm was a repeat test of specimen 2 with the orientation of the bolt heads changed. Only one peak prior to failure of the gap-lock fitting was observed. This peak load of 322 kN occurred at a crosshead displacement of 28 mm. A further 20 mm of displacement was observed prior to failure at 284 kN. The failure mode was a shear failure of the top left hand bolt through a shear plane in the thread. For this test, once the bolt sheared both halves of the bolt were released and there was an immediate loss of all load.

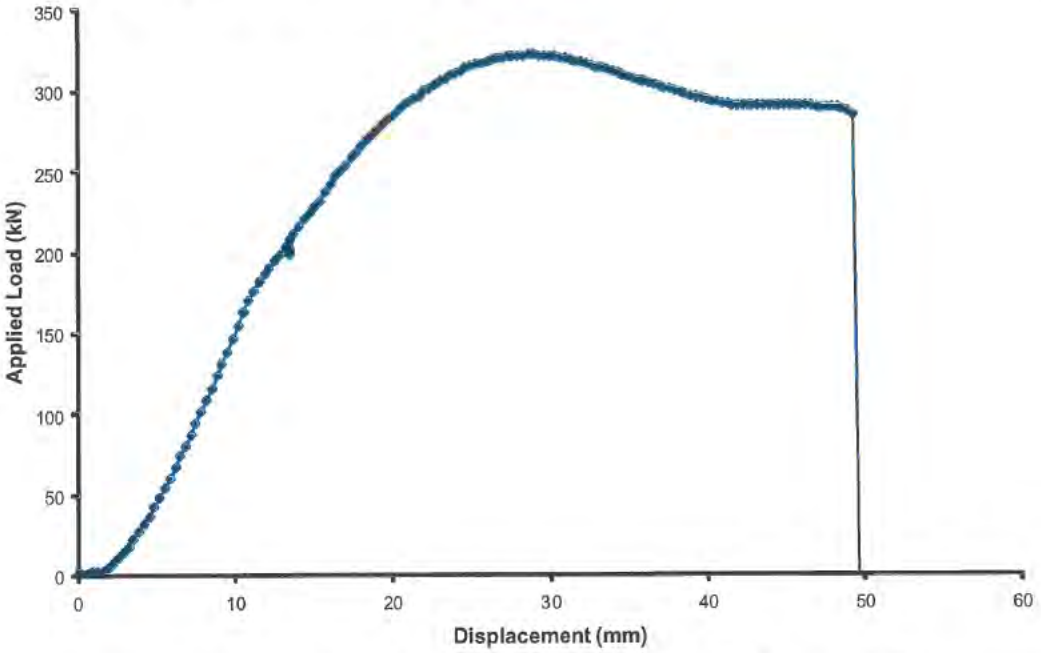

Figure 12 - Specimen 3 - Load vs Cross-Head Displacement Curve

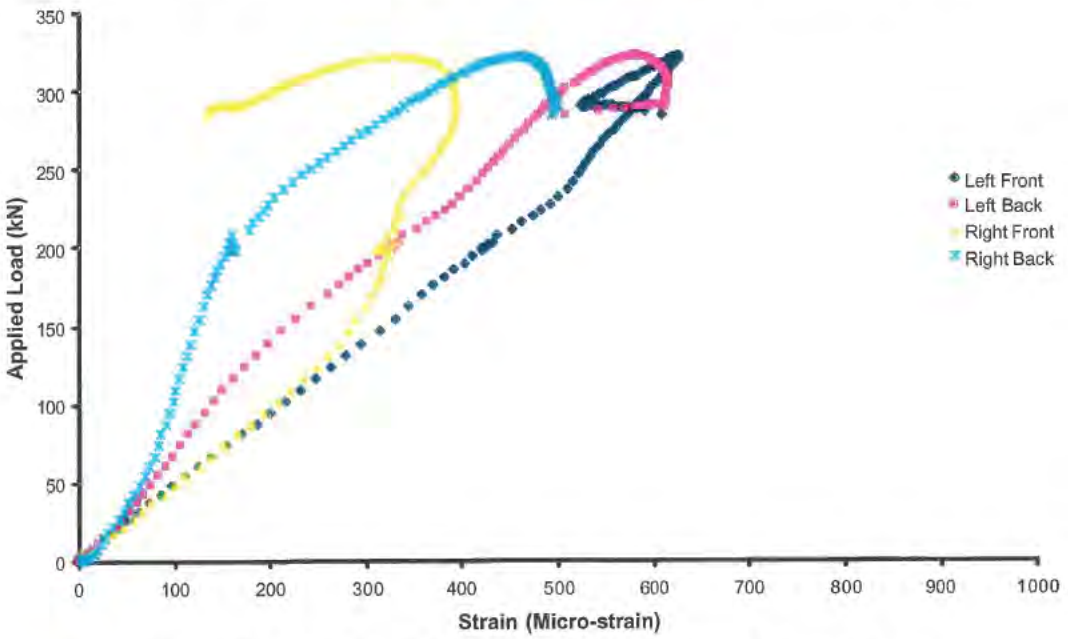

Figure 13 - Specimen 3 - Load-Strain Curves for Strap Plates

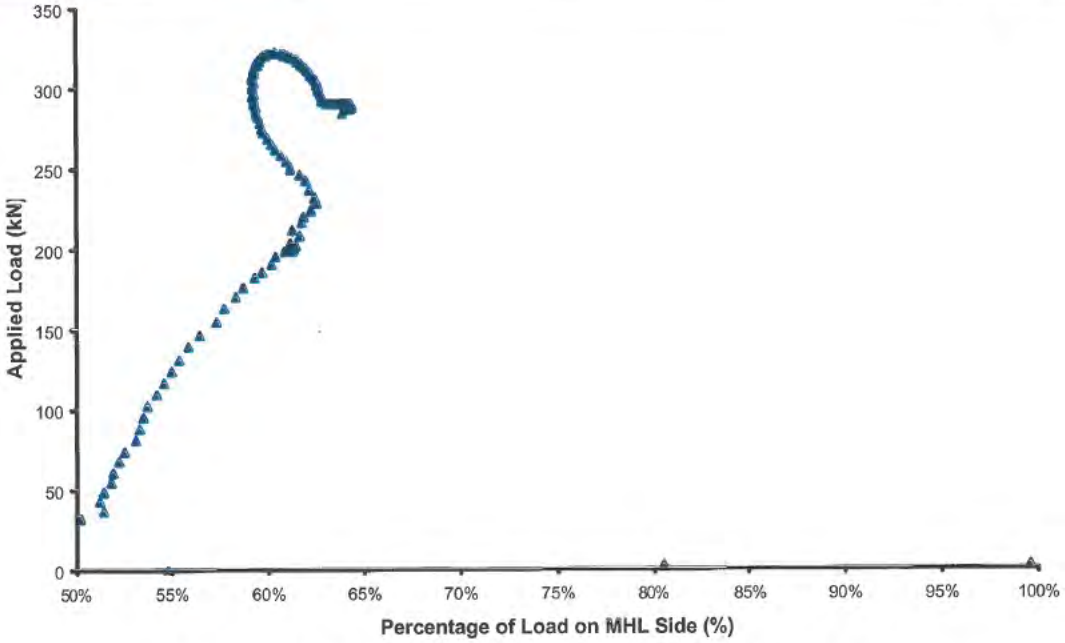

Figure 14 – Proportion of Load carried on MHL Side

The specimen after failure is shown in Figure 15(a). The lateral displacements of the end plate for this test went towards the front, in the direction of the bolt head. The bolt from the lower left side after the test is shown in Figure 15(b). The shear deformation through the threaded section of the bolt shank indicates that the bolt was close to failure.

(a) Failed bolt Missing

(b) Lower bolt, left-hand side

Figure 15 – Failure Mode of Specimen 3

4.1.3 Test #3 - Specimen 1

Specimen 1 incorporated a 110 mm wide end plate exhibited two peaks in the load crosshead movement curve in Figure 15. The first occurred at a displacement of 25 mm at 325 kN. At this point the load fell off to approximately 318 kN until a deflection of about 40 mm. The load then gradually increased until ultimate failure occurred at 395 kN.

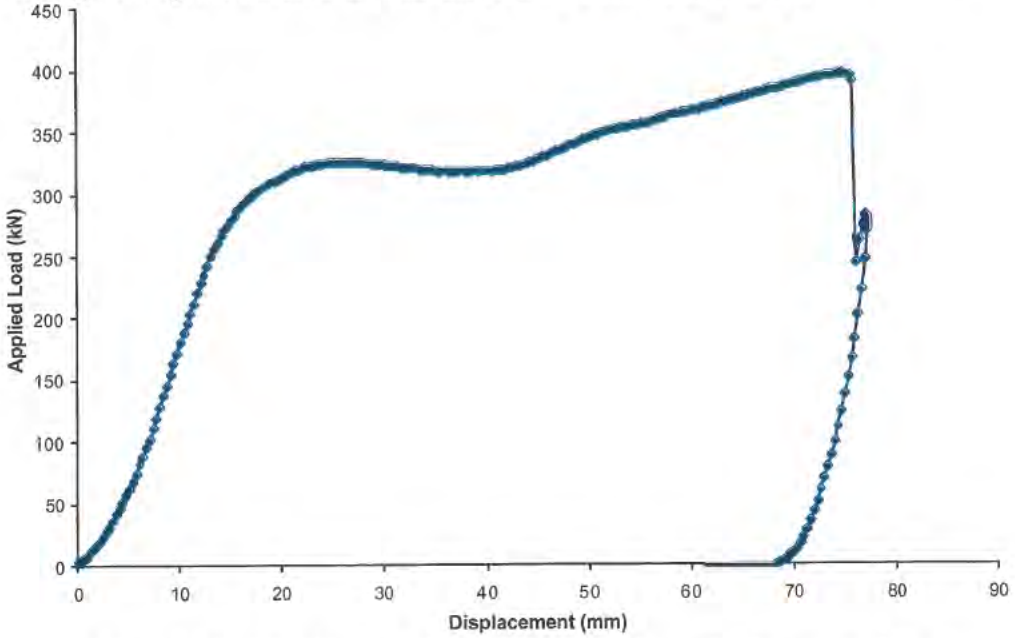

Figure 16 – Specimen 1 - Load vs Cross-Head Displacement Curve

Ultimate failure for specimen 1 involved shear failure of the bottom left-hand bolt through one shear plane. The shear plane that failed passed through the threaded section of the bolt. After failure of the bolt, the bolt head and a short section of the shank remained in the specimen, which continued to carry load in excess of 280 kN. The test was stopped and the specimen was unloaded shortly after the bolt failure.

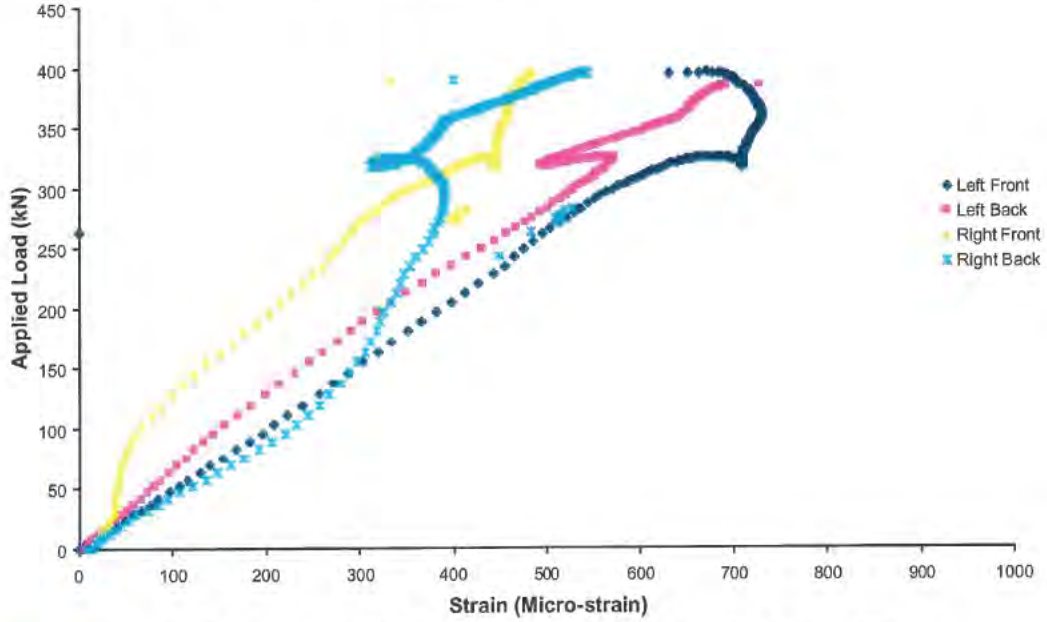

Figure 17 – Specimen 1 - Load-Strain Curves for Strap Plates

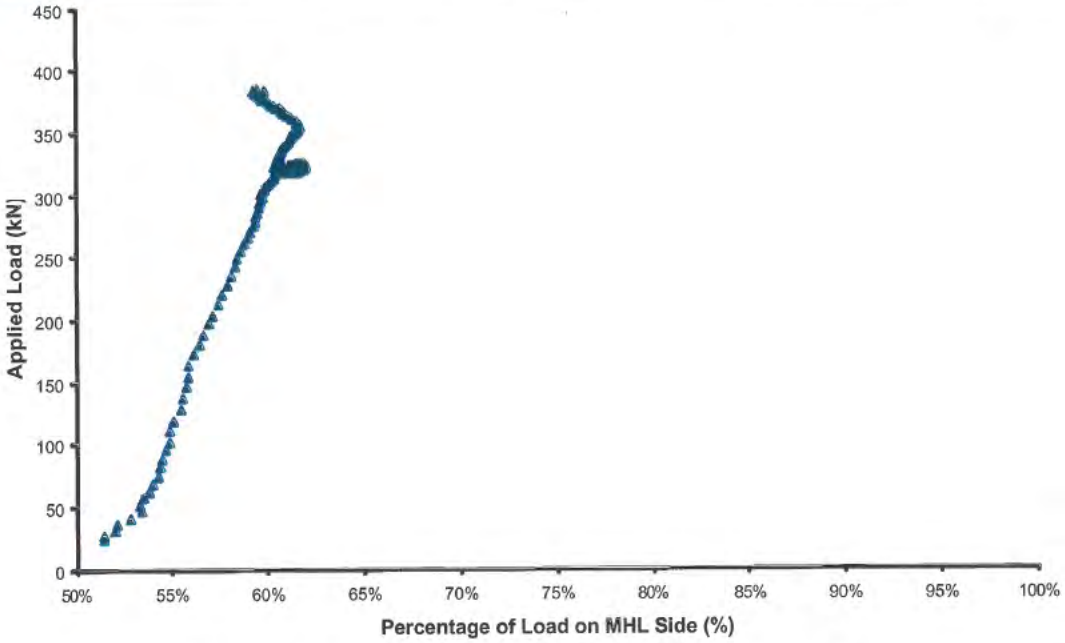

Figure 18 – Proportion of Load carried on MHL Side

The failed specimen is shown in Figure 19. In this photograph the shank of the bolt just below the head can be seen in the end plate while it still transfers load into one of the strap plates. The load being carried by the gap-lock at fitting the time this photograph was taken was 281 kN.

Figure 19 – Failure Mode of Specimen 1

For specimen 1, the lateral deflection of the end plate was towards the rear of the specimen in the direction of the bolt heads.

4.1.4 Test #4 - Specimen 5

Specimen 5 consisted of a 110 mm wide end plate configure for a Type A test, exhibited behaviour similar to specimen 1 with the first peak at 342 at 25 mm. After this peak the load drop until a displacement of 36 mm was reached at which point the load increased until the top left bolt sheared. Again this single failed shear was though one plane through the threaded section of the bolt.

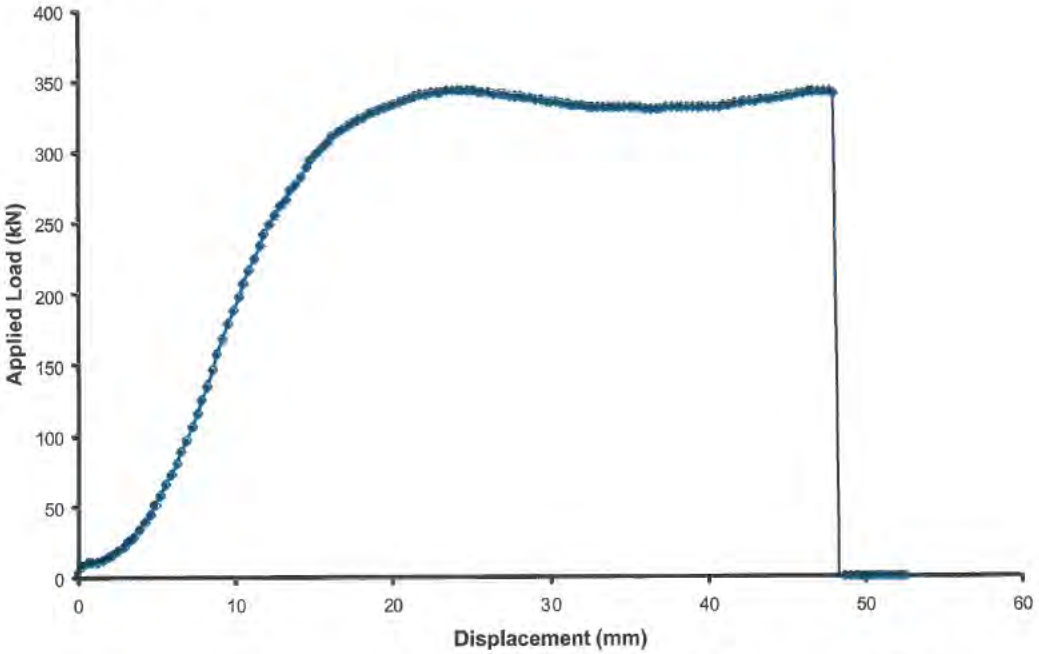

Figure 20 - Specimen 4 - Load vs Cross-Head Displacement Curve

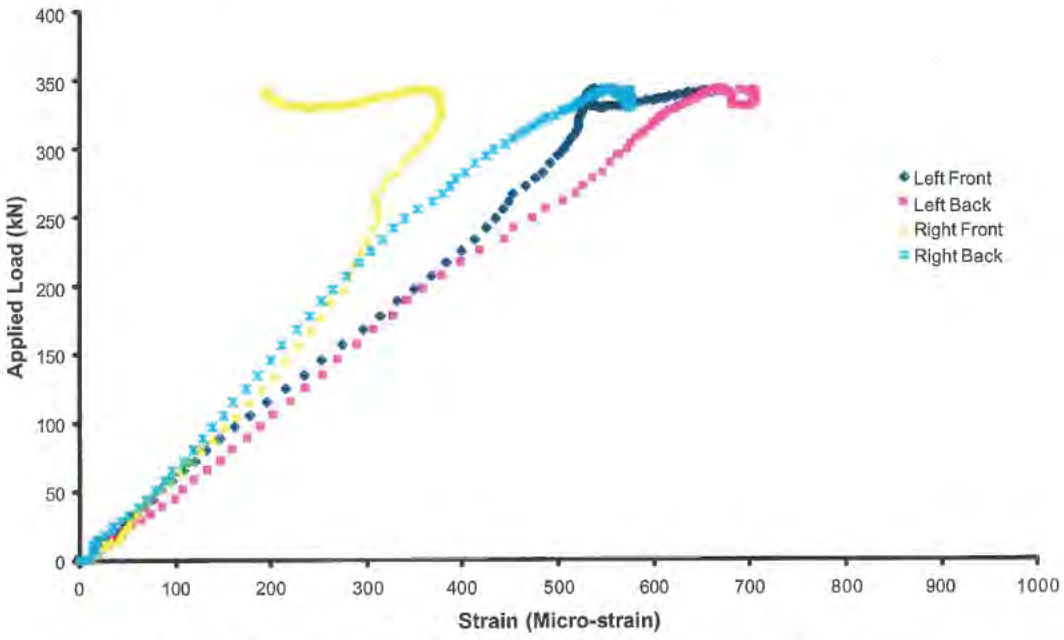

Figure 21 - Specimen 4 - Load-Strain Curves for Strap Plates

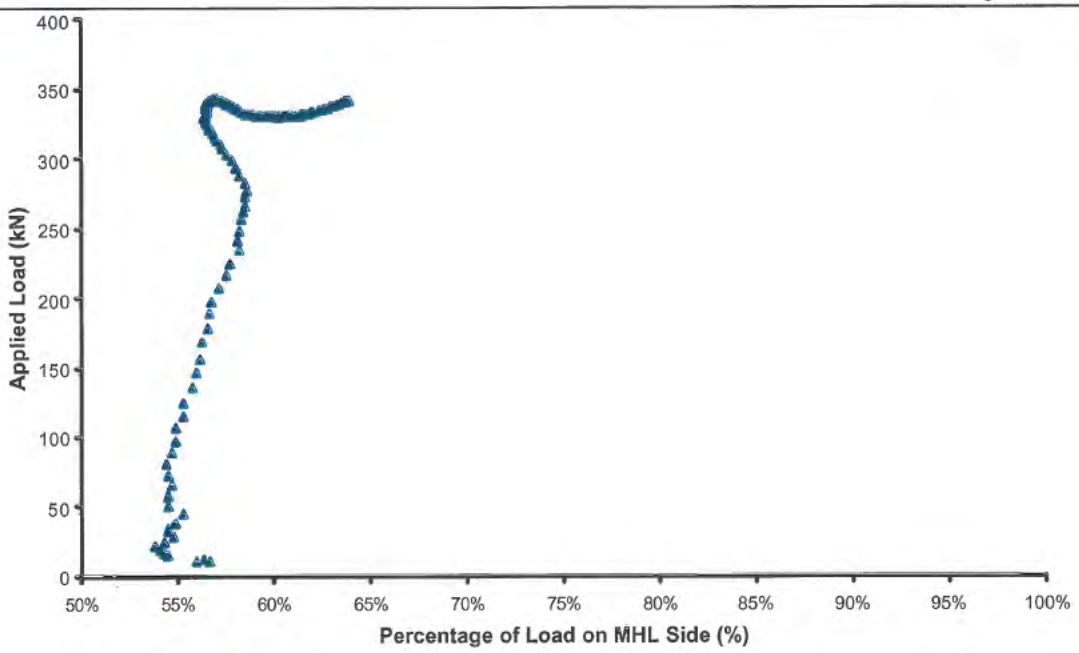

Figure 22 – Proportion of Load carried on MHL Side

Figure 23 shows the specimen just after failure. The deflection of the end plate was forward, towards the bolt heads.

Figure 23 – Failure Mode of Specimen 5

4.1.5 Test #5 - Specimen 4

For Specimen 4 the end plate width was 100 mm with a Type B configuration. To enable the connection to be loose longer bolts were used. Significant yielding of the end plate was observed at an earlier stage than for the type A configuration. The failure mode of the specimen was by plate tearing, which occurred at the top left side and is shown in Figure 27. The failure was relatively sudden, and occurred at a load of 389 kN.

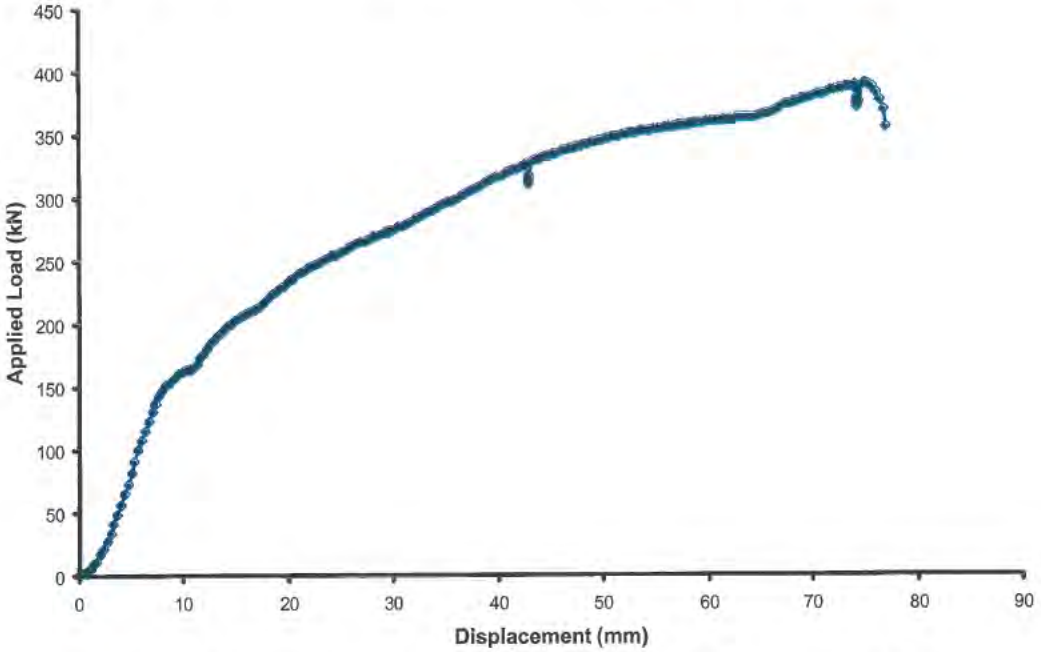

Figure 24 - Specimen 4 - Load vs Cross-Head Displacement Curve

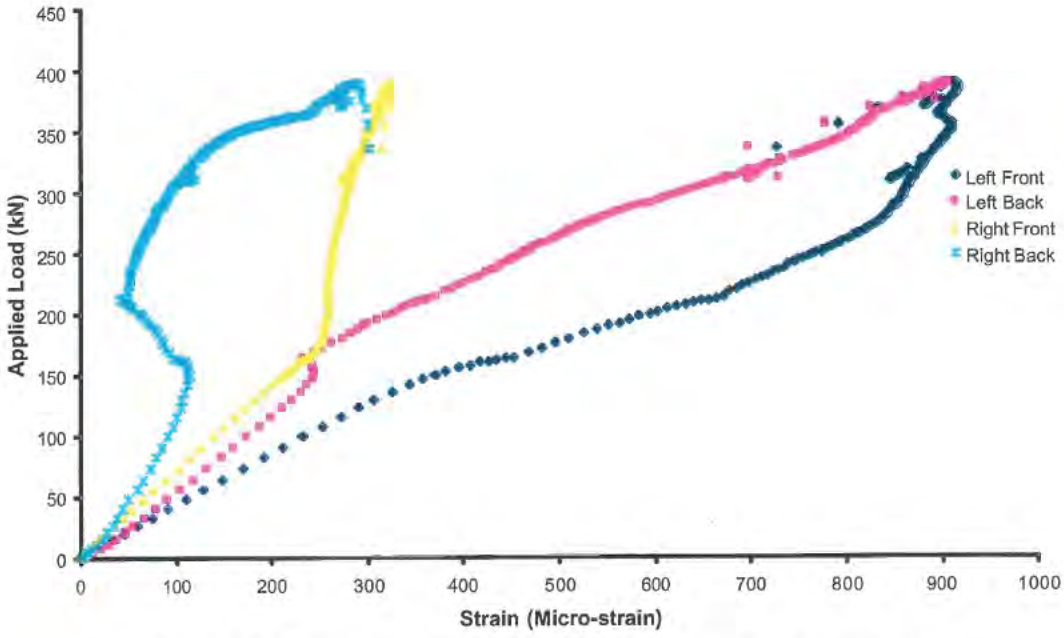

Figure 25 - Specimen 4 - Load-Strain Curves for Strap Plates

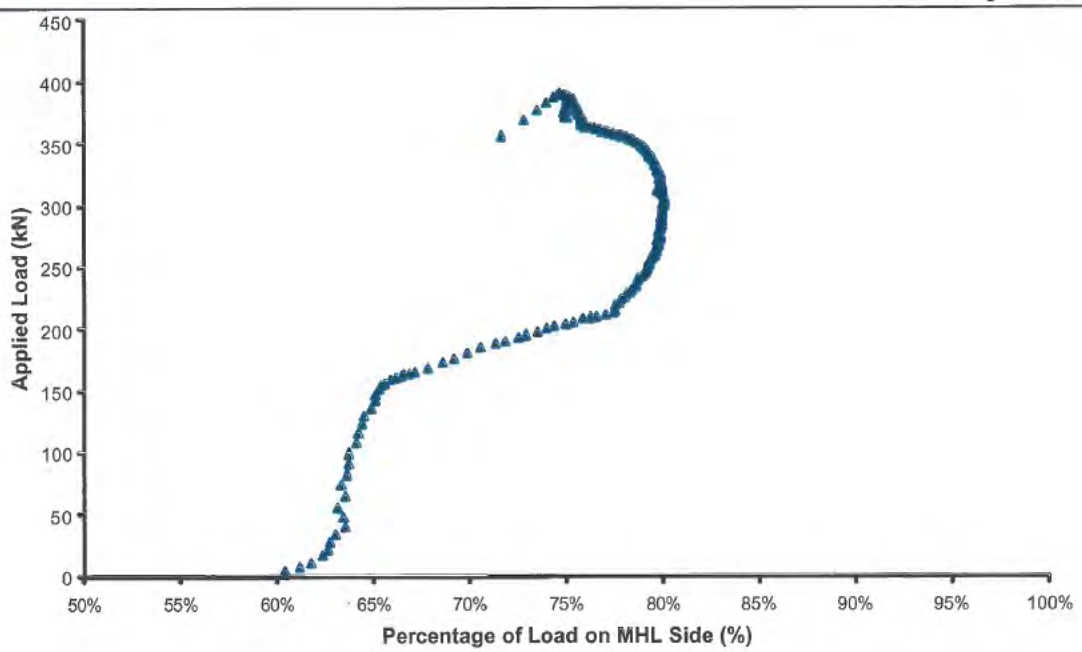

Figure 26 – Proportion of Load carried on MHL Side

For this specimen the lateral deflections of the end plate went towards the rear of the test assembly.

Figure 27 – Failure Mode of Specimen 4

4.1.6 Test #6 - Specimen 9

For Specimen 9 the end plate width was 110 mm with a Type A configuration. The long bolts were selected to ensure that the unthreaded section of the bolt shank passed through both shear planes. The specimen had an initial peak load of 318 kN at 20 mm then lost load until approximately 30 mm beyond which the load progressively increased. The test was stopped at 534 kN due to significant lateral deformations being imposed on the assembly.

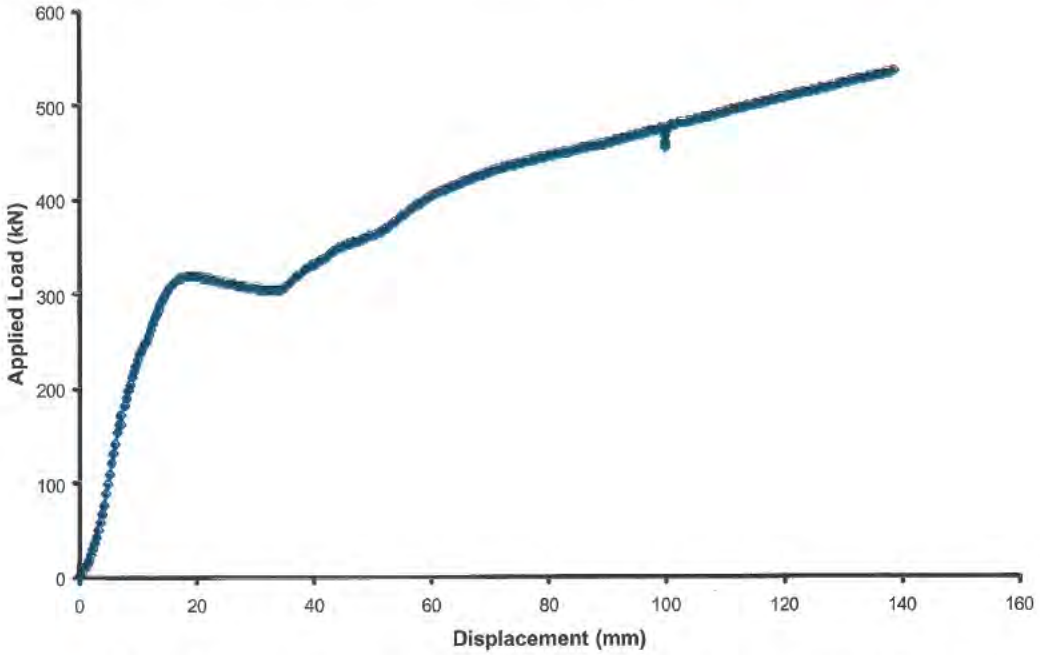

Figure 28 - Specimen 9 - Load vs Cross-Head Displacement Curve

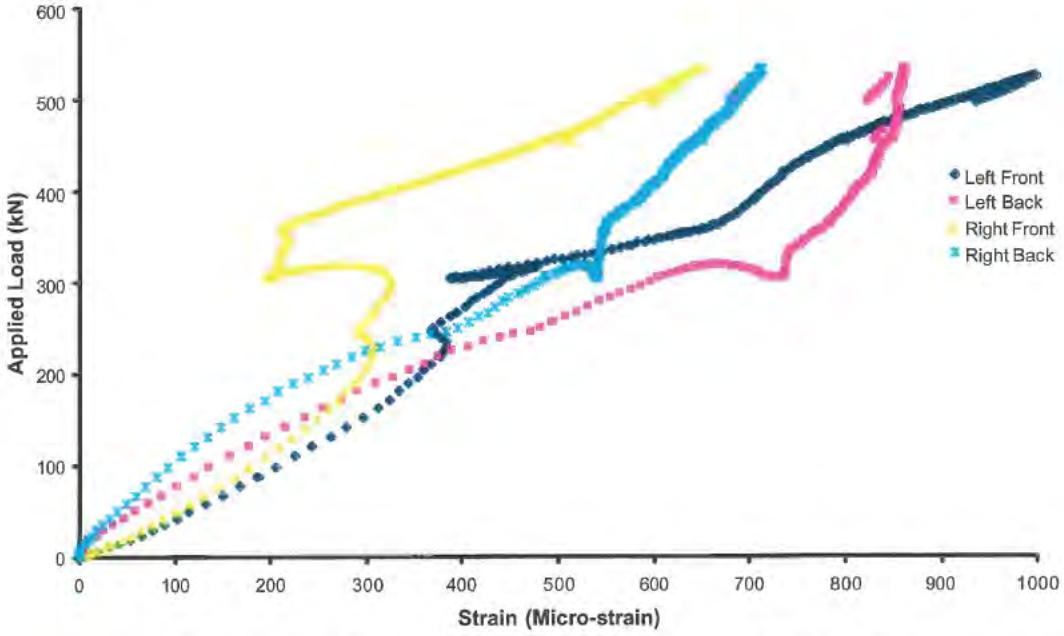

Figure 29 - Specimen 9 - Load-Strain Curves for Strap Plates

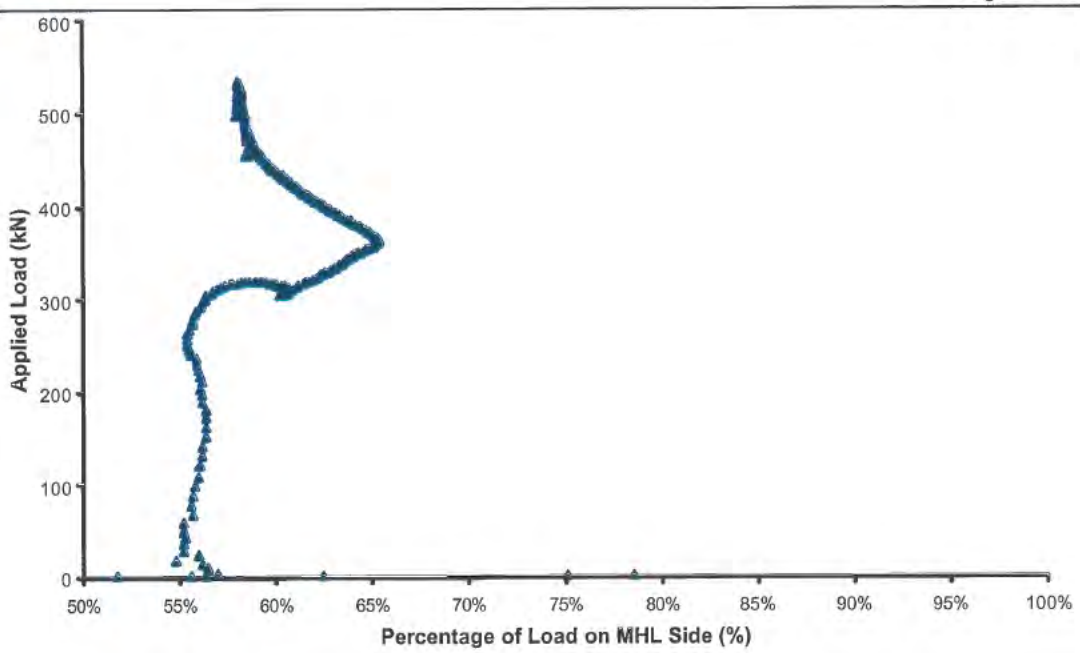

Figure 30 – Proportion of Load carried on MHL Side

The direction of the end plate deflection was forward. As the end plates deformed, the protruding ends of the bolts eventually beared on the chord member as can be seen in Figure 31. As the load increased the deformations of the end plate also increased causing the bolts to pinch the chord members. The test was stopped when these deformations were considered excessive.

Figure 31 – Bolt Ends bearing into Chord Memeber

Upon completion of the test, close inspection of the end-plates revealed significant yielding and tearing at the interface of the corner of the packer plate with the end plate as seen in Figure 32(a). The boltholes on the left side of the test frame also demonstrated significant elongation as shown in Figure 32(b). At the high loads the rotation of the gap-lock fitting resulted in a significant out-of-straightness of the chord member as shown in Figure 33.

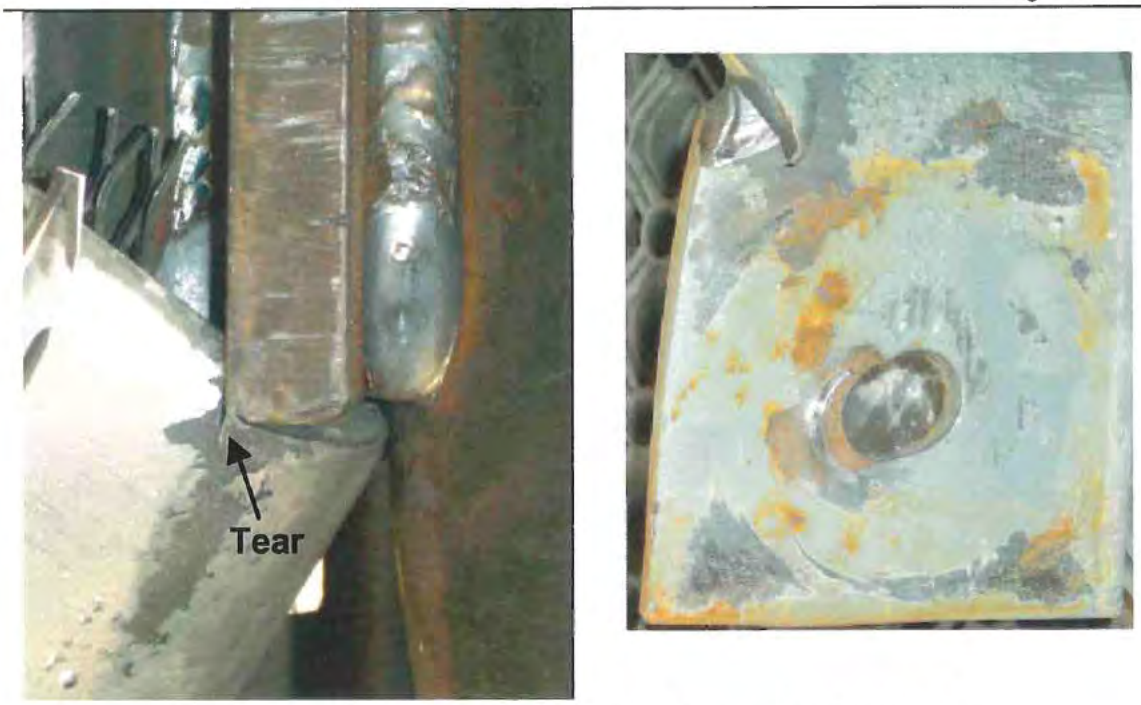

Figure 32 – Tearing of End Plates and Elongation of Bolt Holes

Figure 33 – Specimen at Peak Load

4.1.7 Test #7 - Specimen 6

Specimen 6 had an end-plate width of 100 mm, tested using the Type A configuration, and washers under the nuts. Initially a peak load of 280 kN was reached at 18 mm deflection, at this point the end plates began to yield with the load decreasing significantly as the bottom endplate deflected laterally. At this stage on small lateral deflections were observed at the top end plate (see Figure 37(a)). Once the endplate at the bottom came into contact with the chord member the applied loads began to increase until an ultimate load of 334 kN was reached. As the applied load increased the lateral deflections at the top endplate also increased. The failure mode for specimen 6 was a shear failure of the bottom left hand bolt through one shear plane located in the threaded section of the bolt.

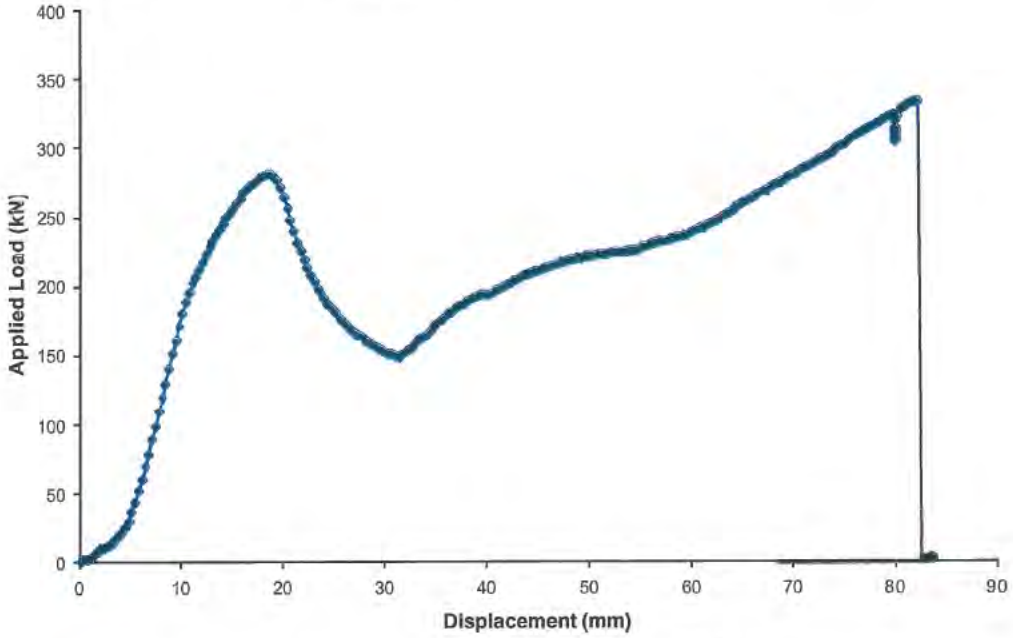

Figure 34 - Specimen 6 - Load vs Cross-Head Displacement Curve

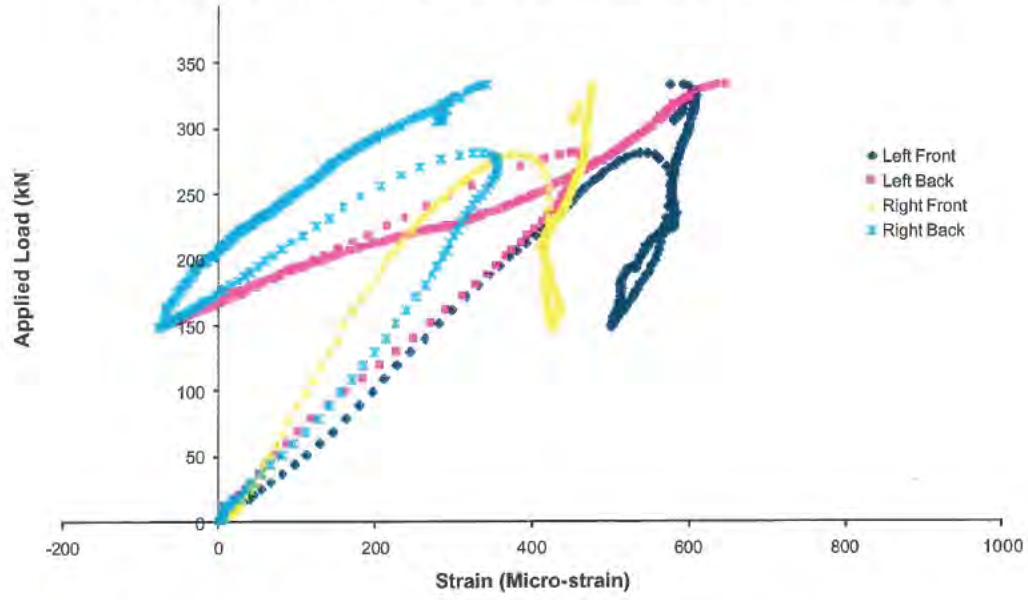

Figure 35 - Specimen 6 - Load-Strain Curves for Strap Plates

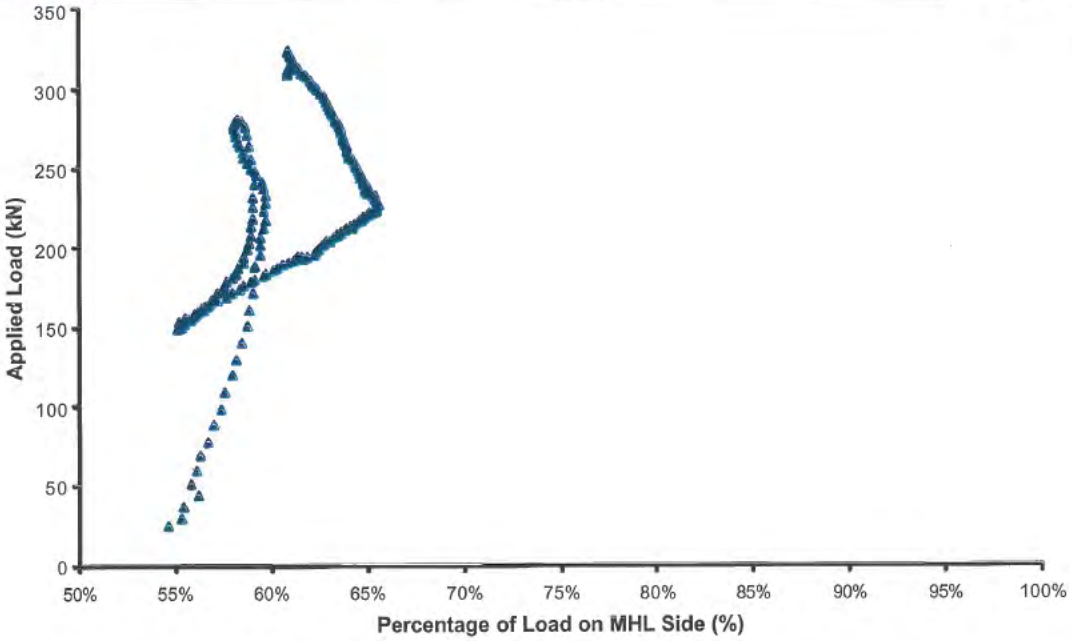

Figure 36 – Proportion of Load carried on MHL Side

The mode of failure is clearly shown in Figure 37(b) with the bolt missing from the fitting. The lateral movement of the end plate was towards the rear of the test assembly. The variation in the deformations of the side of the chord members is shown in Figure 37(c).

(a) Twisting of the bottom End-plate

(b) Missing Bolt

(c) Chord Member Deformations

Figure 37 – Failure Mode Specimen 6

4.1.8 Test #8 - Specimen 7

Tested using the Type B configuration, with an end-plate width of 100 mm specimen 7 was a repeat test of specimen 9 with short bolts. For this test the lateral deflection of the end plates was towards the front of the test rig. The plastic deformations on the bottom chord members at the front was significantly less (Figure 37(c)), thus preventing the significant drop in load observed in Specimen 7. The ultimate load was 326 kN, and occurred when the top left-hand bolt failed through a single shear plane through the thread section of the bolt.

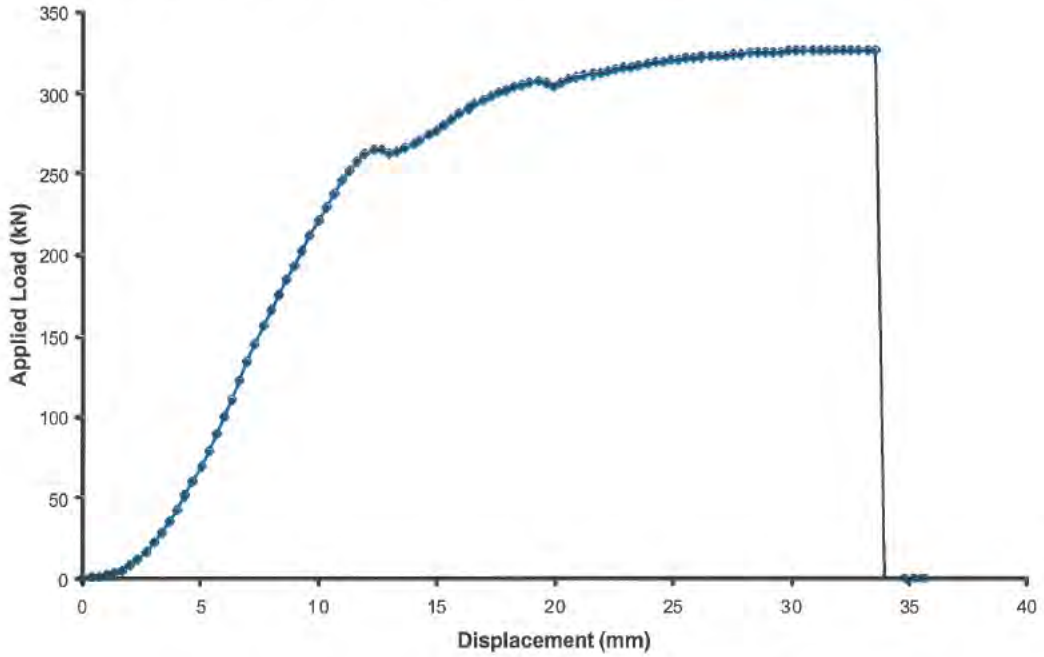

Figure 38 - Specimen 7 - Load vs Cross-Head Displacement Curve

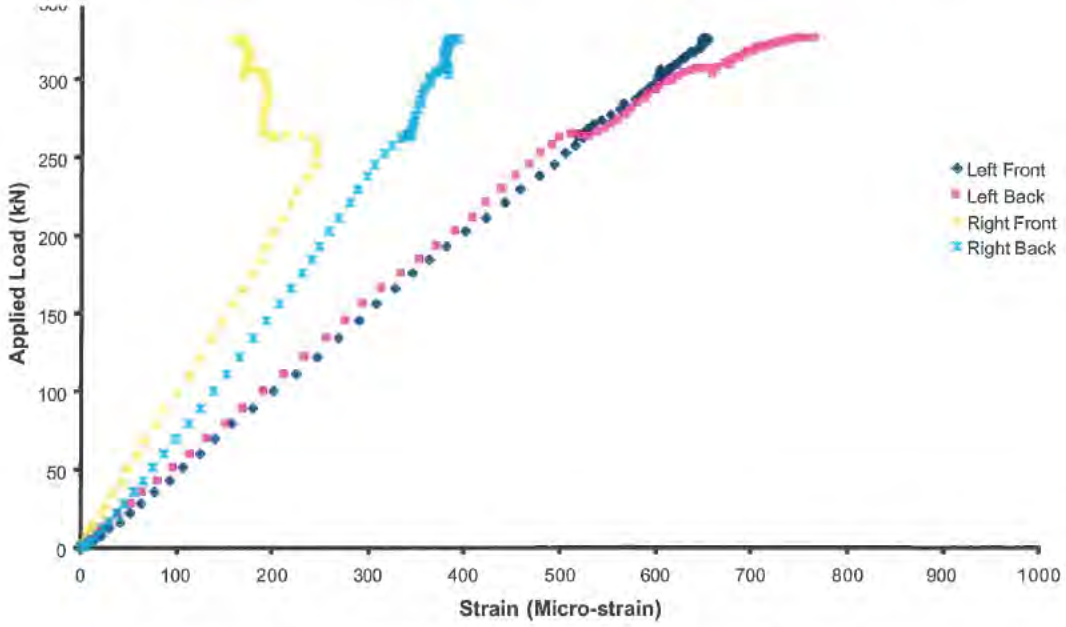

Figure 39 - Specimen 7 - Load-Strain Curves for Strap Plates

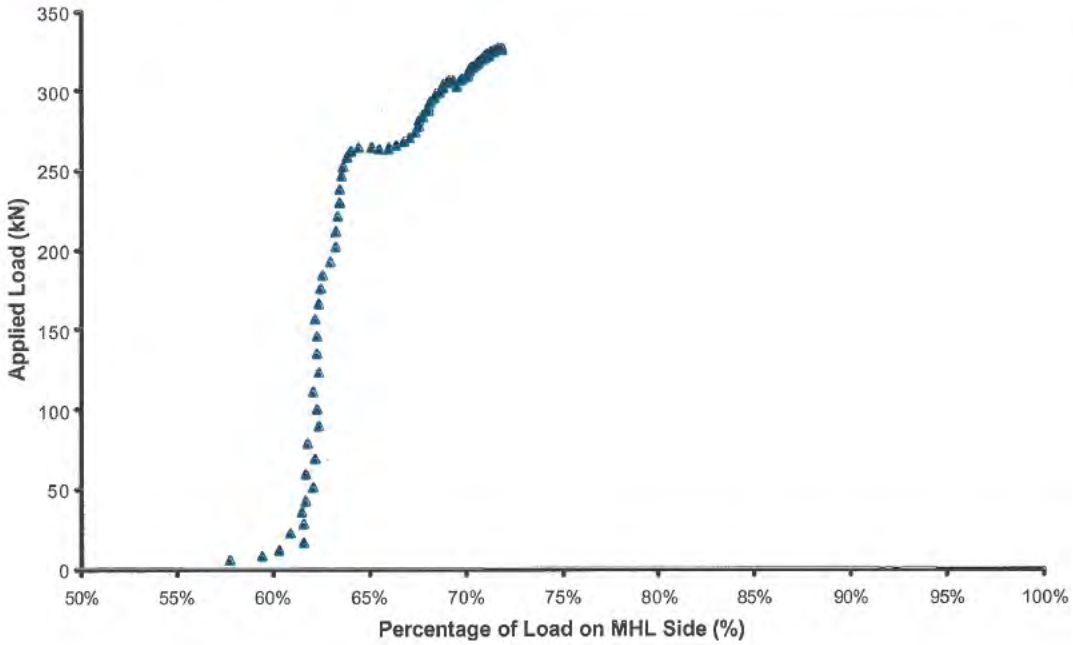

Figure 40 – Proportion of Load carried on MHL Side

The gap in the test configuration Type B allowed for some unrestrained rotation of the end plate under loading see Figure 41, with a gap on the top right and bottom left. It should also be noted that while the bolt length was shorter, 1½ threads still protruded through the nut.

Figure 41 – Rotation of the End Plate

4.1.9 Test #9 - Specimen 8

Specimen 8 consisted of a 110 mm end plate, with long bolts positioned in a manner to ensure that both shear plane passed through the shank of the bolt. The Lateral deflections of the end plates was towards the back of the test rig and as observed for specimen 6 the load dropped significantly at yield until the endplate came into contact with the chord member. From this point the load gradually increased until the test was stopped due to excessive deformations at a load of 514 kN.

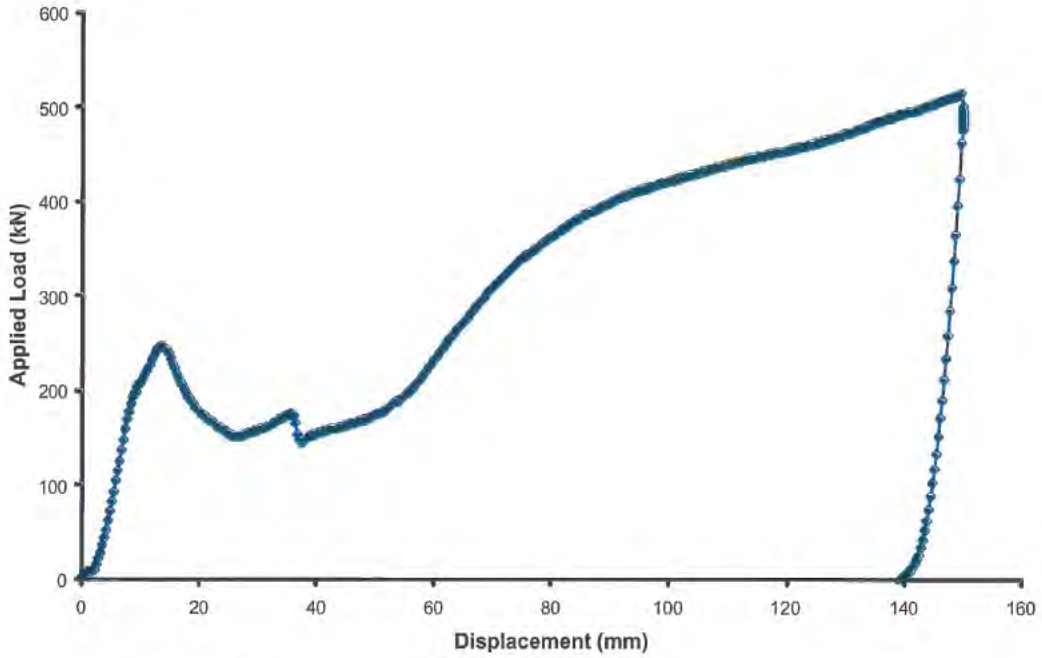

Figure 42 – Specimen 8 - Load vs Cross-Head Displacement Curve

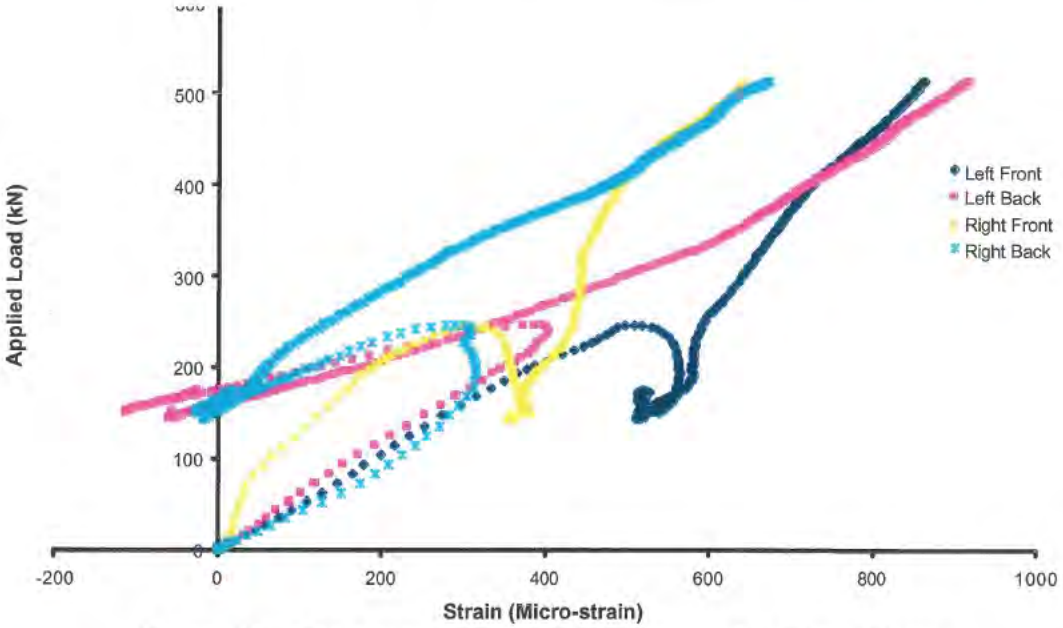

Figure 43 – Specimen 8 - Load-Strain Curves for Strap Plates

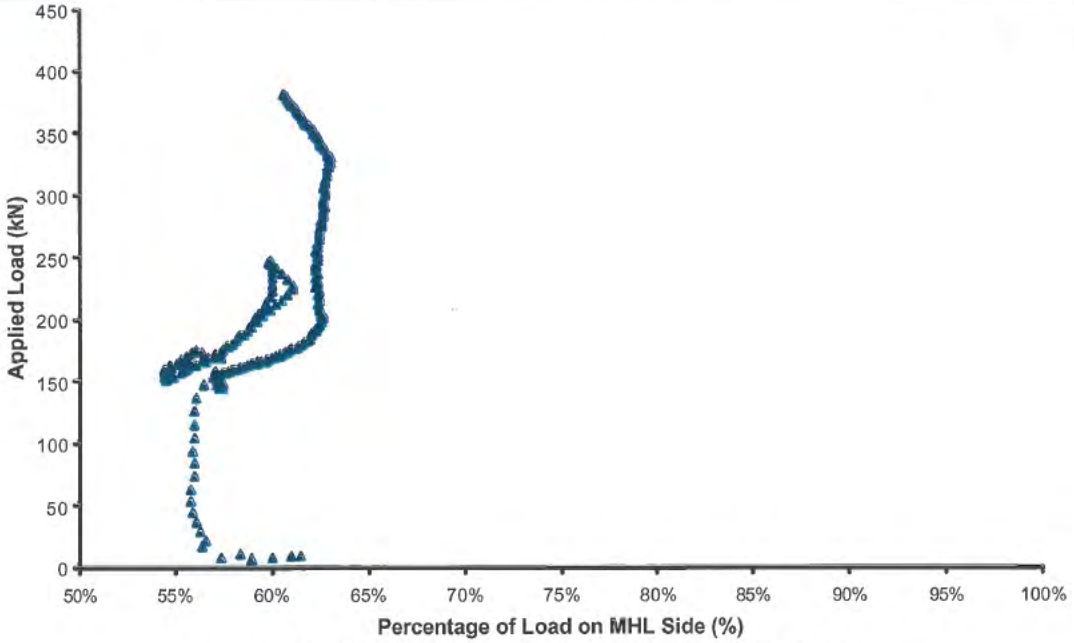

Figure 44 – Proportion of Load carried on MHL Side

To prevent the bolts from bearing into the chord member as experience in Specimen 4 the bolt length was reduced so that 1½ threads protruded out of the nut when fastened. With the bolts shortened the chord member was now pinched by the nuts when the plate had deformed see Figure 45 (b).

(a) Specimen During testing

(b) Pinched Section

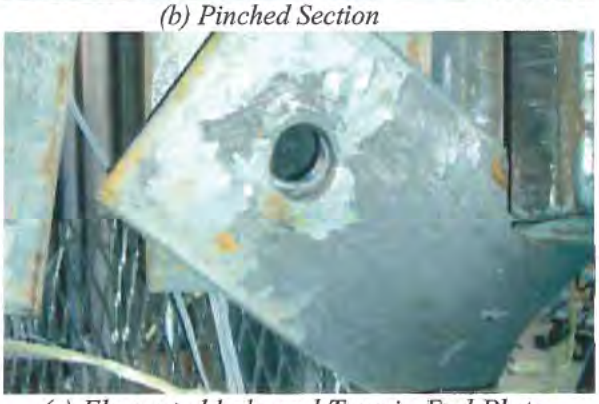

(c) Elongated hole and Tear in End Plate

Figure 45 – Failure of Specimen 8

For both specimen 6 and specimen 8 the end plate at the bottom experienced significant more early rotation as a result of the reduced restraint provided by the chord member. As a result when the loads were dropping the rear strap plates had a net compressive load as shown by the strain load curves (Figure 35 and Figure 43).

4.2 *Summary*

The ultimate load obtained for each test and the observed mode of failure are presented in Table 4. Also presented are the peak loads applied to the bolts on the MHL side of the fitting, these loads are determined using proportional loads and the applied load as presented for each specimen.

Table 4 – Summary of Results

Specimen #	Ultimate Load kN	Failure Mode*	Load MHL Side (kN)
1	395.9	Bolt shear failure	230.5
2	361.8	Bolt shear failure	203.9
3	322.0	Bolt shear failure	195.5
4	389.8	Plate tensile tearing	291.4
5	342.8	Bolt shear failure	218.4
6	333.6	Bolt shear failure	200.7
7	326.2	Bolt shear failure	234.4
8	513.5	Large deformation	295.5
9	534.0	Large deformation	310.0

* the bolt shear failure always occurred in the threaded section of the bolt

For a comparison of the behaviour of all the tests Figure 46 gives the load vs. crosshead displacement curves.

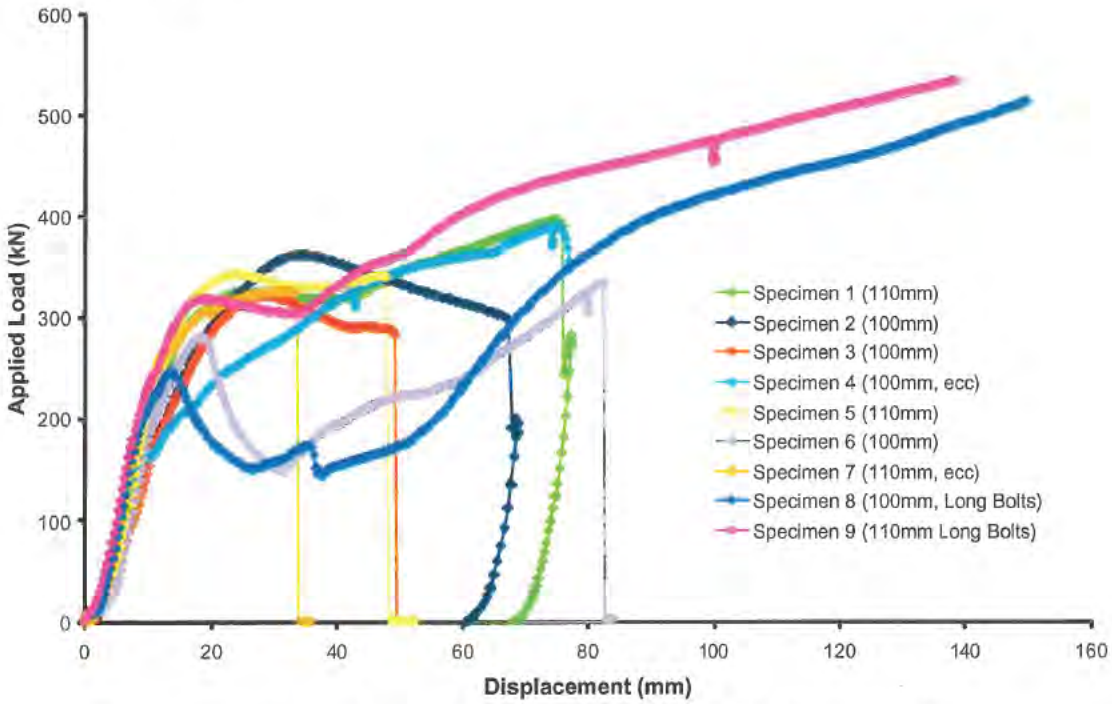

Figure 46 – All Specimens - Load vs. Cross-Head Displacement Curves

For all tests the end plates experienced significant plastic deformations, with the shear failure of the bolts being the dominant failure mode. The shear failure was always through one shear

plane located in the threaded section of the bolt. When the long bolts were used so that the shear planes passed through the shank of the bolt, the specimens either tore the end plate or were stopped when the load exceeded 510 kN and was experiencing large deformations.

The typical failure mode of the bolts is demonstrated in Figure 47, were all the failed bolts are shown. In every case, one shear plane through the threaded section of the bolt was observed.

Figure 47 – Failed bolts

The last three tests viz. Specimens 6,7 and 8 demonstrated that significant restraint was provided by the chord member. When the end plate was prevented from rotating between the members of the chord the post yield behaviour demonstrated a small loss in load prior to strain hardening or failure of the bolt. When the restraint against rotation was reduced then significant losses in load were observed prior to increasing loads and ultimate failure. Regardless of the restraint of the end plate the ultimate load at which the bolt failed was similar.

Signed

A Wheeler
Approved Signatory
Centre for Construction Technology and Research

Appendix A -

Specimen 1

During Test

Specimen at Failure

End plates after testing.

Specimen 2

During Test

At failure

End plates after testing.

Specimen 3

During test

End plate during test

After Failure

End plates after testing

Specimen 4

During test

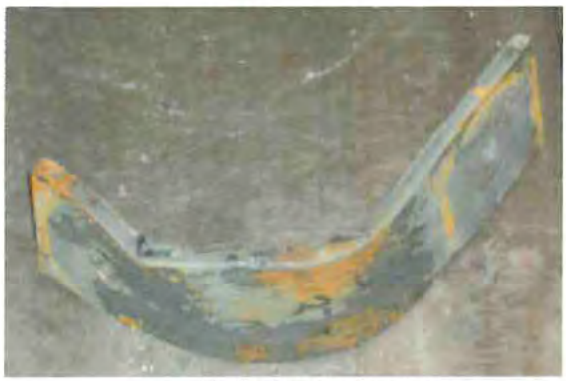

End plates after test

Failed Endplate

Specimen 5

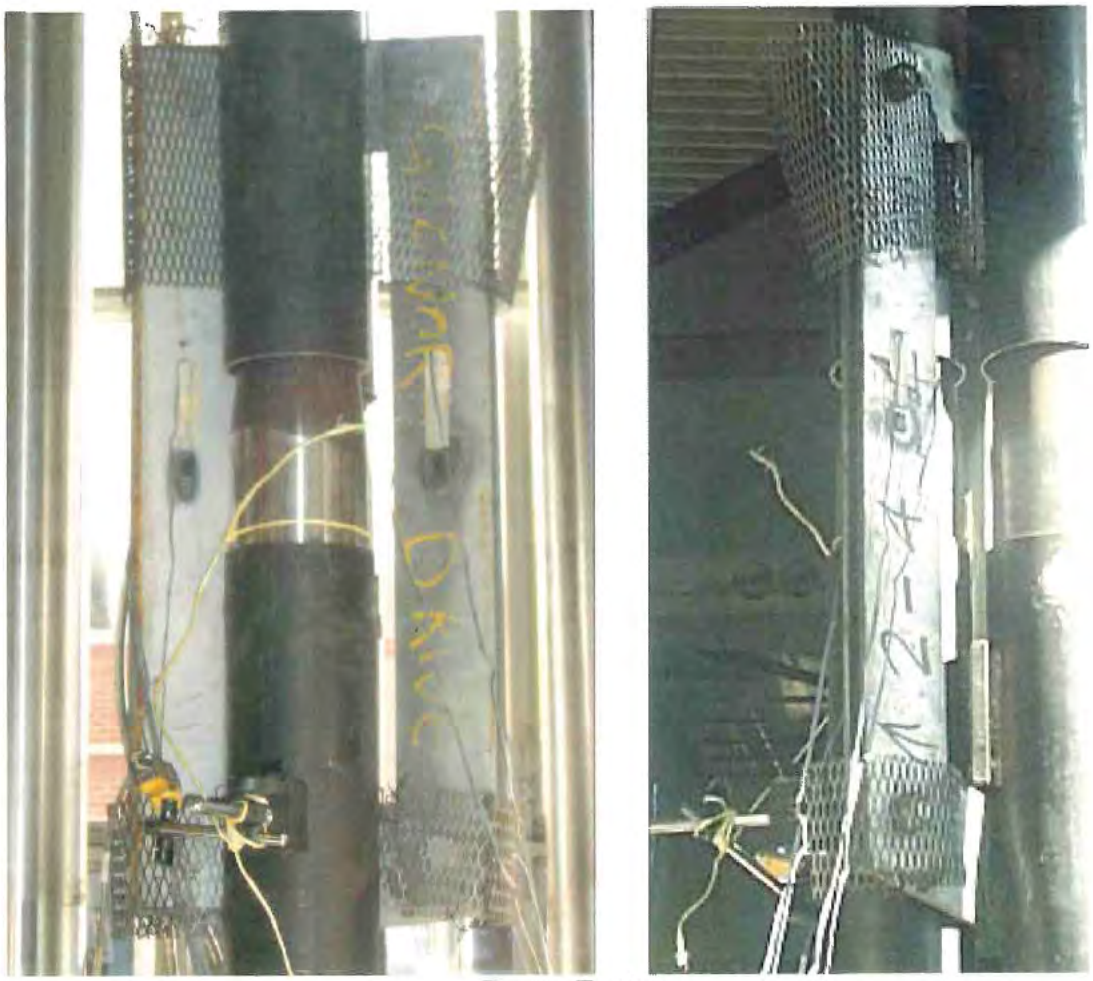

During Testing

End plates after test

Specimen 6

During test

End plate deformations

End plate at failure

End plates after test

Specimen 7

During test

Twisting of the end plate

End Plate after test

Specimen 8

During test

Deformations at peak load

End plates after test

Tearing of end plate

Specimen 9

During test

Endplate at peak load

End plates after test